Solid-state electrolytes for beyond lithium-ion batteries: A review

Hasna Aziam [a], Badre Larhrib [b], Charifa Hakim [c], Noha Sabi [d], Hicham Ben Youcef [a,**], Ismael Saadoune [c,e,*]

[a] High Throughput Multidisciplinary Research (HTMR), Mohammed VI Polytechnic University (UM6P), Lot 660 Hay Moulay Rachid, Ben Guerir, Morocco
[b] CNRS/UNIV Pau & Pays Adour/E2S UPPA, Institut des Sciences Analytiques et de Physicochimie pour l'Environnement et les Matériaux (IPREM), UMR5254, 64000 Pau, France
[c] IMED, Faculty of Science and Technology- Cadi Ayyad University (UCA), Av. A. El Khattabi, P.B. 549, Marrakesh, Morocco
[d] Institute for Applied Materials – Energy Storage Systems (IAM-ESS), Karlsruhe Institute of Technology, Hermann-von-Helmholtz-Platz 1, 76344 Eggenstein-Leopoldshafen, Germany
[e] Technology Development Cell (Techcell), Mohammed VI Polytechnic University, Lot 660, Hay Moulay Rachid Ben Guerir, 43150, Morocco

ARTICLE INFO

Keywords:
Solid-state electrolytes
Potassium-ion batteries
Calcium-ion batteries
Magnesium-ion batteries
Zinc-ion batteries
Aluminum-ion batteries

ABSTRACT

Safe energy storage technique is prerequisite for sustainable energy development in the future. Designing Solid-State Electrolytes exhibiting high ionic conductivity, good electrochemical performances, high mechanical/thermal stability, compatible electrolyte/electrode interface is the main concern for developing the next-generation rechargeable batteries. This review presents the state of the art of Solid-State Electrolytes for beyond lithium-ion batteries, mainly, for Sodium-ion batteries, Potassium-ion batteries, Calcium-ion batteries, Magnesium-ion batteries, Zinc-ion batteries, and Aluminum-ion batteries. The main aspects of SSEs, including the synthesis processes, the physico-chemical properties, and the electrochemical performance, are emphasized.

1. Introduction

The lithium-ion battery (LIB) technology available in the market relies on the use of liquid electrolytes which consist of a lithium salt dissolved in one or a combination of several organic solvents. Although this configuration delivers good electrochemical properties, it may induce serious hazards which threaten our safety due to electrolyte leakage, flammability of its components, dendrite formation, and undesirable side reactions between the electrolyte and electrodes [1,2]. To overcome these issues, several strategies were suggested such as using additives like flame retardants (e. g. trifluoropropylene carbonate, hexamethoxycylcotriphosphazene, Trimethyl phosphate, triethyl phosphate), or additives to improve the solid electrolyte interphase (abbreviated as SEI) (e. g. vinylene carbonate, and methyl cinnamate), or using ionic liquids as electrolytes or as solvents [3]. Nevertheless, solid-state electrolytes (SSEs) were distinguished as an effective solution for safe batteries. In fact, SSEs demonstrate good mechanical properties, facile processing, high thermal/chemical stabilities, superior flame retardation, long shelf life, high flexibility, and high stability in large electrochemical voltage window. Electrolyte leakage and flammability at high temperature are not problematic when using SSEs [4]. Furthermore, SSEs play simultaneously the role of an electrolyte and a separator. However, SSEs suffer from poor ionic conductivity (IC) at room temperature (RT) and high interfacial resistance between electrodes and SSEs [5,6]. The main concern of researchers is meeting the challenges and the requirements of this technology and succeeding to develop high IC SSEs for the Next-Generation Batteries. Three main categories of SSEs were classified based on their chemical composition that consist of inorganic, organic, and hybrid SSEs. The first includes for example sulphide-based inorganic electrolytes, β-Alumina electrolytes, and NASICON electrolytes. The second category contains polymer electrolytes, gel polymer electrolytes, and plastic crystal electrolytes. Last, hybrid electrolytes are the combination of both organic and inorganic SSEs. Several SSE formulations were investigated for all-solid-state Lithium batteries (ASSLB) [7–17]. For example, polymer solid state electrolytes using polyethylene oxide (PEO) as matrix were widely studied. Large interest was dedicated to PEO as polymeric matrix since 1973 due its high dielectric constant, high lithium salt dissolving ability,

* Corresponding author. IMED, Faculty of Science and Technology- Cadi Ayyad University (UCA), Av. A. El Khattabi, P.B. 549, Marrakesh, Morocco.
** Corresponding author. High Throughput Multidisciplinary Research (HTMR), Mohammed VI Polytechnic University (UM6P), Lot 660 Hay Moulay Rachid, Ben Guerir, Morocco.
E-mail addresses: hasna.aziam@um6p.ma (H. Aziam), badre.larhrib@univ-pau.fr (B. Larhrib), charifahakim@gmail.com (C. Hakim), noha.sabi2@kit.edu (N. Sabi), Hicham.benyoucef@um6p.ma (H. Ben Youcef), i.saadoune@uca.ma (I. Saadoune).

low cost, good stability, and compatibility with the cathode material. However, PEO suffers from low ionic conductivity at room temperature and limited electrochemical window. Therefore, organic fillers, Li-free inorganic fillers (i.e., C_3N_4, BN, ..), and Li-conductive inorganic fillers (such as $Li_{10}GeP_2S_{12}$, $Li_7La_3Zr_2O_{12}$) were proposed as a strategy to solve these problems. For instance, Li-conductive inorganic fillers improve the mechanical properties and Li transference number [18]. Many challenges are hindering the development of ASSLB. First, the cost of ASSLB is relatively very high and estimated to be around $100/kWh where the SSE costs 35% of the total price [19]. Mainly, Lithium precursors are very expensive as well due to the low abundance of lithium in earth crust (0.006 wt%) and the uneven geographical distribution in few countries such as Chile, China, Australia, Argentina, and Portugal [20]. Second, good contact between the SSE and electrodes is difficult to achieve. During battery operation, the charge/discharge process induces volume change of the electrode material which severely causes loss of contact and formation of cracks leading to battery failure. Third, Lithium dendritic growth was also reported as an issue facing this technology where it induces short-circuits and as consequence, battery failure. To remedy to this, adding fillers or building an artificial SEI layer were proposed as effective solutions [9]. Moreover, achieving high IC at room temperature, low electronic conductivity, controlling the interfacial impedance and grain-boundary resistance, expanding the working voltage window, chemical stability with Li metal are as well great challenges to overcome.

This review summarizes the state-of-art of SSEs for beyond lithium-ion batteries. To this end, we focus on the research carried on SSEs for for Sodium-ion batteries (SIBs), Potassium-ion batteries (KIBs), Calcium-ion batteries (CIBs), Magnesium-ion batteries (MIBs), Zinc-ion batteries (ZIBs) and Aluminum-ion batteries (AIBs). The properties of the chemical elements Li, Na, K, Mg, Ca, Zn, and Al in term of their abundancy in earth crust, their average redox voltage potential versus standard hydrogen electrode (SHE), and their hydrated ion radius are depicted in Fig. 1. Li, Na and K are very reactive elements which highly induces safety hazards. Multivalent metal ions like Mg^{2+}, Ca^{2+}, and Al^{3+} suffer from low diffusion and reaction kinetics [21,22]. In addition, Zn suffers from dendrite growth during extended cycles, self-discharge problems by sustained consumption of electrolyte, and formation of irreversible substances (i.e., ZnO) [22]. All these issues could be solved by switching from liquid electrolytes to SSEs. Therefore, the most abundant element in this group is aluminum (~8.23%) and the less abundant is Lithium with only 0.0018%. However, lithium shows the lowest redox potential which involves the highest energy density (~ 3.04 V vs. SHE), followed by potassium, calcium, sodium, magnesium, aluminum, and last, zinc. On the other hand, the volumetric capacities of post-lithium technologies are greater than Li except for Na and K. Thus, the combination of these above-mentioned features leads to a new stage for reliable, low-cost, and safe energy storage system.

The number of published papers on SSEs for LIBs and beyond has increased lately. Looking at the published papers from 2010 to May 30th, 2022 (Fig. 2), researchers showed great interest and focus on developing SSEs as promising alternatives for replacing flammable liquid electrolytes. This review has dedicated special attention to the preparation process, thermal behaviour, IC, and efficiency tests of the reported SSEs in a half or full cell configuration. To the best of our knowledge, this is the first report reviewing SSEs for several battery technologies beyond LIBs.

2. Solid-state electrolytes for SIBs

In SIBs, safety hazards are more serious than in LIBs because sodium is highly reactive in contact with humidity and air. Therefore, all-solid-state SIBs is an attractive safe alternative for the future of the battery industry. Nonetheless, it is a challenging technology as well because it requires a high Na^+ ion conductor SSEs and good contact between SSEs and electrodes. Side reactions between metallic sodium and the SSE block charge transfer and increase interfacial resistance [23,24]. Several types of SSEs were proposed as convenient candidates for efficient all-solid-state SIBs [8–63].

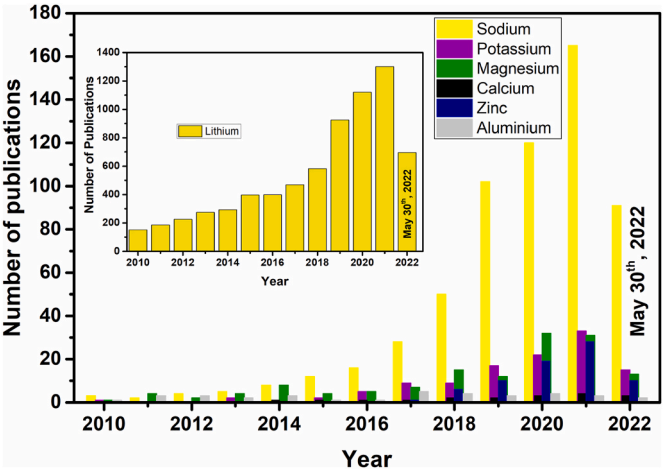

Fig. 2. Number of articles related to SSEs (lithium and beyond) published from 2010 to May 30th, 2022 (obtained from Web of Science).

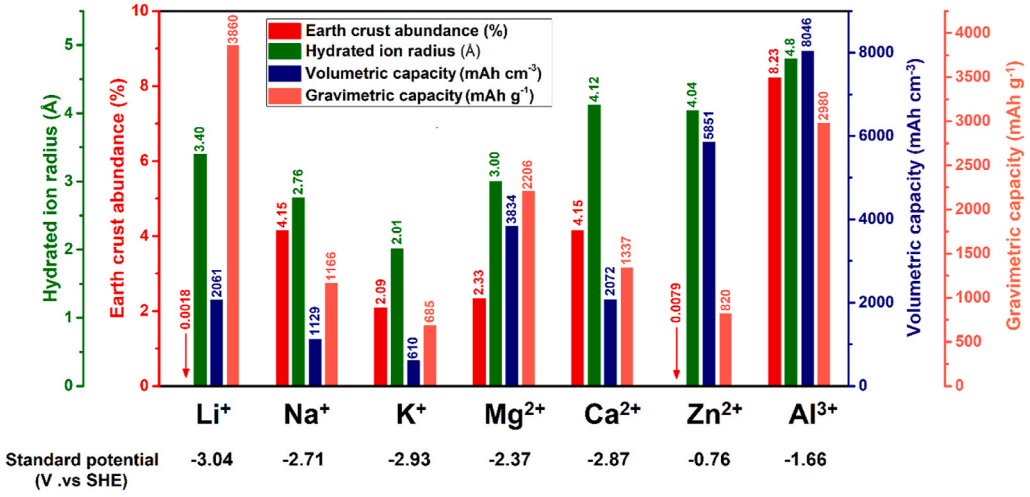

Fig. 1. Properties of the chemical elements Li, Na, K, Mg, Ca, Zn, and Al, and their corresponding theoretical capacities [21,22].

2.1. Inorganic solid electrolytes

Sulphide SSEs show high IC at RT ($\geq 10^{-3}$ S cm^{-1}) thanks to the weak binding energy between Na^+ ions and high polar S^{2-} anion. They also demonstrate interesting mechanical properties, which preserve good solid-solid contact with the change of volume upon charge-discharge process. Moreover, grain-boundary resistance is reduced by cold pressing the sulfide SSEs without further calcination at high temperatures [26]. In 2012, Hayashi et al. [27] synthesized a sulphide glass-ceramic electrolyte Na_3PS_4 for all-solid-state sodium sulfur batteries. The preparation process was carried out using mechanochemical technique where Na_2S and P_2S_5 were ball-milled for 20 h, heated at 270 °C and then at 420 °C. This thermal treatment enables going from glass phase to well crystallized Na_3PS_4. This material showed a high sodium IC of 2×10^{-4} S cm^{-1} at RT which is attributed to the reduction of grain-boundaries. The prepared electrolyte was tested using Na–Sn and TiS_2 electrode materials at 25 °C with 0.013 mA cm^{-2} current density. It delivers a reversible capacity of more than 90 mAh g^{-1} for 10 cycles (See Fig. 3a). The remarkable electrochemical performances shown here are attributed to the high-temperature treatment that reduced the grain-boundary resistance of the Na_3PS_4 and therefore, enhance the contact between the electrode and the solid electrolyte. In 2014, the same group [28] reported enhanced conductivity of the glass ceramic electrolyte Na_3PS_4 and its electrochemical properties were studied in a full cell configuration: $Na_{15}Sn_4/Na_3PS_4/NaCrO_2$. This study is the first to report a 3 V all-solid-state SIBs using sodium layered oxide cathode. The preparation of Na_3PS_4 consisted of mixing Na_2S (high purity, 99.1 wt%) and P_2S_5 with a molar ratio of 75% and 25%, respectively. Na_3PS_4 shows the highest conductivity around 4.6×10^{-4} S cm^{-1} when the milling time was set to 1.5 h and the calcination at 270 °C for 1 h. The full cell was cycled at 0.013 mA cm^{-2} current density and 25 °C. As shown in Fig. 3 b, capacities of 130 mAh g^{-1} and 80 mAh g^{-1} were delivered during the first and the 3rd charges, respectively. The capacity is decreasing with the excessive charge/discharge cycles due to the increase in the cell resistance (Fig. 3c).

Wenzel et al. [29] reported the efficiency of Na_3PS_4 and Na-β″-Al_2O_3 as SSEs against metallic sodium. The measured IC values at 25 °C are 2.1 mS cm^{-1} and 0.04 mS cm^{-1}, while the electronic conductivities are 3×10^{-9} S/cm^{-1} and 6×10^{-12} S cm^{-1} for Na_3PS_4 and Na-β″-Al_2O_3, respectively. In 2016, Chu et al. [23] studied the effect of Cl doping in $Na_{3-x}PS_{4-x}Cl_x$ superionic conductor and evaluated its efficiency as solid electrolyte in $TiS_2/Na_{3-x}PS_{4-x}Cl_x/Na$ cell. Na_2S, P_2S_5, and NaCl precursors were mixed, pressed into pellets, and then densified using spark plasma sintering to reduce porosity in the resulting solid electrolyte. At 303 K, Pure Na_3PS_4 demonstrates IC of 0.05 mS cm^{-1}, which is low compared to that obtained for x = 6.25% (~1.14 mS cm^{-1}) whereas the activation energies are 317 meV vs. 249 meV, respectively. Furthermore, $Na_{3-x}PS_{4-x}Cl_x$, with a doping ratio of x = 6.25%, delivered a capacity of 80 mAh g^{-1} for 10 cycles with 100% efficiency (Fig. 4a). Therefore, the good performance of the doped electrolyte is attributed to the salting effect, which induces the formation of an electronically insulating, but ionically conductive SEI. In 2017, Zhang et al. [30] investigated the effect of the crystal structure of Na_3SbS_4 on the ionic diffusion. For this purpose, cubic and tetragonal Na_3SbS_4 (denoted as *c*- and *t*-Na_3SbS_4, respectively) were synthesized. Indeed, the IC measurements confirmed that at RT, *c*- Na_3SbS_4 shows higher value than *t*-Na_3SbS_4 (2.8 mS cm^{-1} vs. 1.77 mS cm^{-1}). *c*- Na_3SbS_4 is the high temperature polymorph of *t*-Na_3SbS_4, which explains the improvement

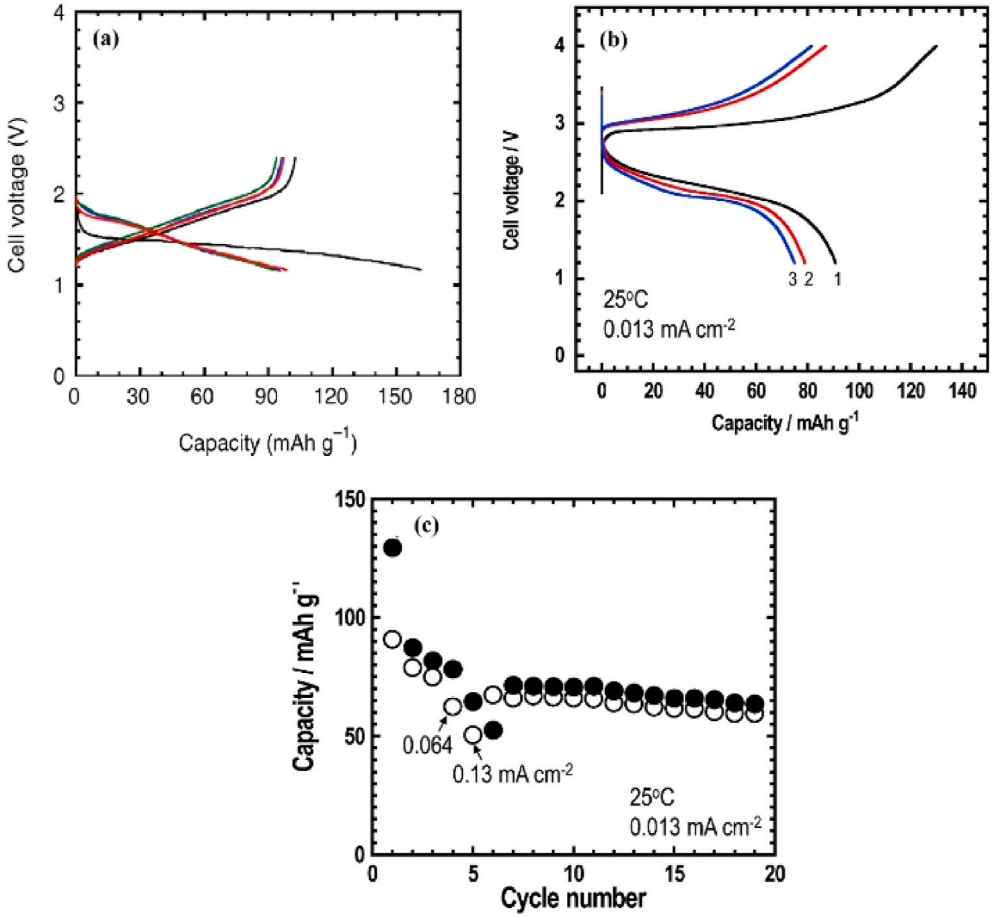

Fig. 3. **(a)** Voltage vs. capacity profile of Na–Sn/Na_3PS_4 glass-ceramic/TiS_2 (Copyright 2012, Nature) [27]. **(b)** First three Voltage vs. capacity curves, **(c)** Capacity vs. cycle number of $Na_{15}Sn_4$/cubic-Na_3PS_4 glass–ceramic/$NaCrO_2$ cell (Copyright 2014, Elsevier) [28].

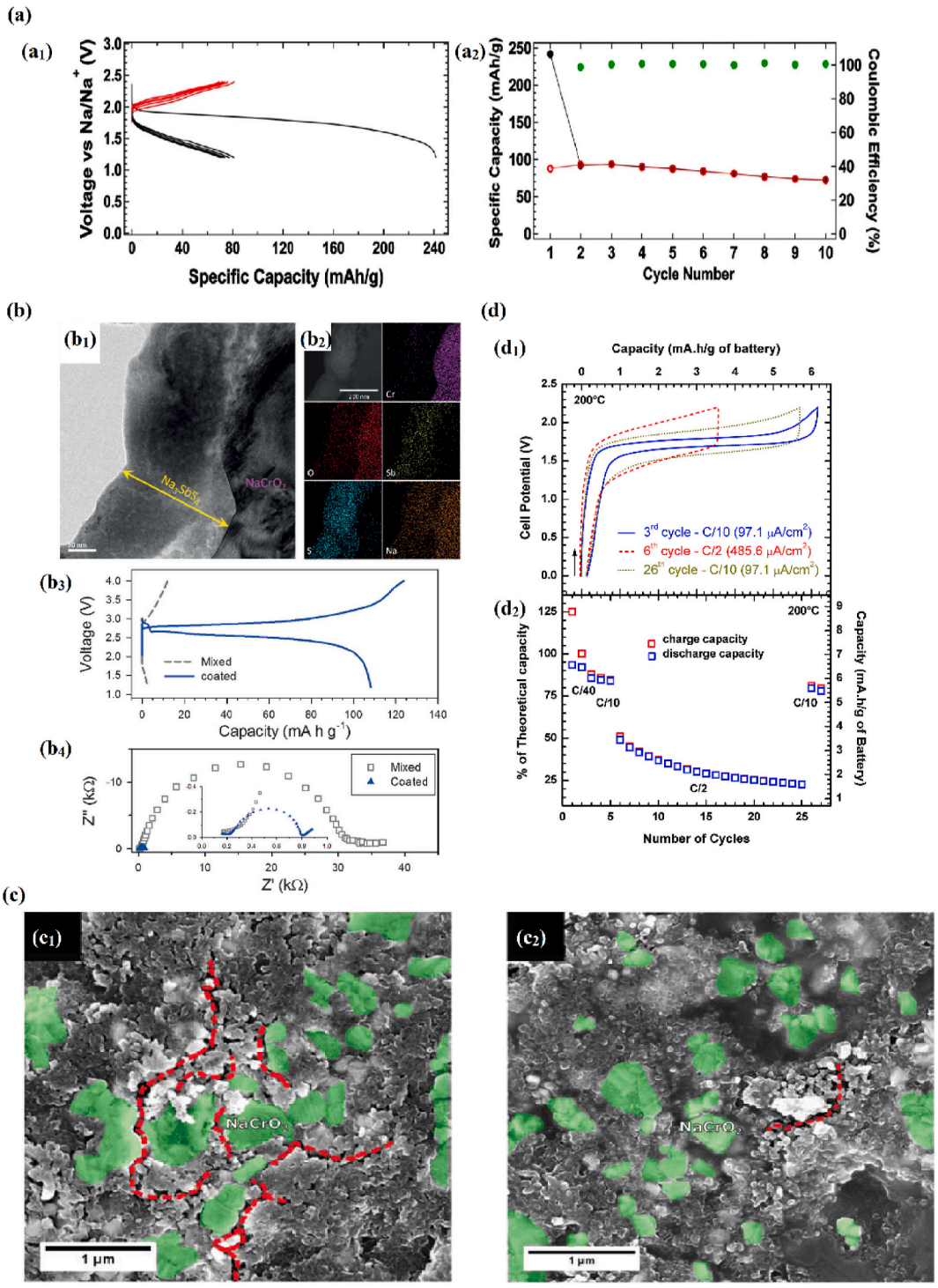

Fig. 4. **(a_1)** Voltage vs. capacity profile of TiS_2/t-$Na_{2.9375}PS_{3.9375}Cl_{0.0625}$/Na full cell at C/10, **(a_2)** Capacity and CE vs. cycle number [23] (Copyright 2016, Nature). **(b_1)** HRTEM image of Na_3SbS_4-coated NCO, **(b_2)** TEM images Na_3SbS_4-coated NCO and EDS mapping, **(b_3)** First cycle vs. voltage, **(b_4)** Nyquist plots of NCO/Na-Sn [32] (Copyright 2016, Wiley). **(c)** SEM images of the **(c_1)** mixed and **(c_2)** impregnated cathode mixtures [33] (Copyright 2014, Elsevier). (d_1) Charge-discharge curves at C/2 and C/10 during the 3rd, 6th and 26th cycles and (d_2) capacity retention at 200 °C [34] (Copyright 2017, RSC).

of the IC. The cubic phase was assembled with $NaCrO_2$ and $Na_{15}Sn_4$ as positive and negative electrodes, respectively, delivering capacity of 250 mAh g^{-1} over 1–3 V at 0.064 mA cm^{-2} and 0.13 mA cm^{-2} current densities.

Yu et al. [31] worked on series $Na_3P_{1-x}As_xS_4$ ($0 \leq x \leq 1$) as SSEs for all-solid state sodium ion batteries. Stoichiometric amounts of Na_2S, P_2S_5, and As_2S_5 were ball-milled for 15 h with 510 rpm speed, and then pelletized before heat treated at 270 °C for 2 h. The electrolyte with $x =$ 0.38 shows the highest Na-ion conductivity which is around 1.46 mS cm^{-1} at RT. The electrochemical behaviour of $Na_3P_{0.62}As_{0.38}S_4$ was evaluated in the cell configuration of Na–Sn/$Na_3P_{0.62}As_{0.38}S_4$/TiS_2. At 0.02C current rate, discharge capacities of 175 mAh g^{-1} and 110 mAh g^{-1} were reached in the first and ninth cycles, respectively when the electrochemical cycling was performed at 80 °C. In 2016, Banerjee et al. [32] studied a dry air stable sulfide-based SSE Na_3SbS_4 showing significant IC of 1.1 mS cm^{-1} at RT and an activation energy (E_a) of 0.20 eV

Na_3SbS_4 was prepared using solid-state reaction by mixing Na_2S and SbS_3 precursors proceeded by an annealing at 500 °C. The SSE was coated on $NaCrO_2$ electrode using solidified solution of Na_3SbS_4 (aqueous or methanol-based). Unlike the conventional preparation of composite electrodes where the SSE is mixed with the electrode material and pressed, this process enables intimate contact between the two components. The coating was confirmed using HRTEM and EDXS elemental mapping as depicted in Fig. 4 b_1 and **b_2**. A uniform layer of Na_3SbS_4 with 200 nm thickness was successfully coated on the cathode particles. The Na_3SbS_4-coated $NaCrO_2$ shows similar discharge capacity obtained using liquid electrolyte (~108 mAh g^{-1}) whereas the physically mixed electrodes show a negligible discharge capacity (Fig. 4 b_3). Moreover, the Nyquist plots (Fig. 4 b_4) demonstrate that the mixed electrode undergoes higher charge transfer resistance at the solid electrolyte-electrode interface compared to the Na_3SbS_4-coated $NaCrO_2$. Hayashi et al. [24] synthesized $Na_{3-x}Sb_{1-x}W_xS_4$ sulphide solid electrolytes, where stoichiometric amounts of Na_2S, Sb_2S_3, WS_2, and S were ball-milled at 510 rpm for 5–30 h. Then, the mixture was calcined in argon flow at 275 °C for 1.5–18 h $Na_{2.88}Sb_{0.88}W_{0.12}S_4$ demonstrates the highest IC close to 3.2×10^{-2} S cm^{-1}.

Another inorganic solid electrolyte type was reported by Duchêne et al. [33] in 2017. This research group first investigated a 3 V all-solid-state SIBs using inorganic $Na_2(B_{12}H_{12})_{0.5}(B_{10}H_{10})_{0.5}$ electrolyte. For the synthesis of the solid electrolyte, both raw materials $Na_2B_{12}H_{12}$ and $Na_2B_{10}H_{10}$ were ball-milled and then, calcined under vacuum at 270 °C for 12 h. Later, two different preparation methods for mixing $NaCrO_2$ cathode and the prepared electrolyte were developed for comparison. For the first method; labelled as mixed cathode; the cathode powder, electrolyte and conductive carbon were ground with respect to 70 w.t%, 20 wt%, and 10 wt%, respectively. For the second; labelled as impregnated $NaCrO_2$; it consists of dissolving $Na_2(B_{12}H_{12})_{0.5}(B_{10}H_{10})_{0.5}$ in methanol followed by the dispersion of cathode powder in the solution. Afterwards, the drying of the resulting mixture under vacuum at 270 °C is an important step to ensure the crystallization of the SSE. The electrochemical efficiency of the prepared solid electrolytes was evaluated in a half-cell configuration with Na metal and $NaCrO_2$ cathode. A reversible capacity of 80 mAh g^{-1} was delivered at different current rates C/n (n = 20, 10, 5) using the impregnated electrolyte whereas the mixed electrolyte shows severe capacity fading in the ten first cycles. The authors claim that capacity fading here results from loss of contact between the electrolyte-electrode rather than the decomposition of the SSE. The contact quality in both solid electrolytes was studied using SEM (Fig. 4c) where the $NaCrO_2$ particles embedded in the electrolyte were observed. Several cracks were detected mainly in the case of the $NaCrO_2$ with mixed electrolyte whereas smooth surface was observed for $NaCrO_2$ with impregnated electrolyte. Moreover, the impedance spectroscopy measurements conducted at the fully charged cells have shown that the different impedance contributions are lower in the impregnated electrolyte compared to the mixed one. As result, these data confirm that the enhancement of the cathode-electrolyte interface during preparation is essential for efficient and stable electrochemical performance.

NASICON materials were also reported as inorganic SSE for SIBs[18–24]. Masquelier et al. [34] investigated the electrochemical properties of the SSE $Na_3Zr_2Si_2PO_{12}$ (abbreviated as NZSP) at 200 °C in a full cell configuration with $Na_3V_2(PO_4)_3$ (abbreviated as NVP) as cathode and anode. The electrode consisted of 25% of NVP, 60% of NZSP, and 15% of Carbon Super P. The assembly of the solid-state battery was carried according to Park Plasma Sintering technique (SPS) which relies on pressing the layers at 50 MPa and then sintering at 900 °C for 10 min. The IC values of $Na_3Zr_2Si_2PO_{12}$ and $Na_3V_2(PO_4)_3$ at 200 °C were equal to 1.5×10^{-3} S cm^{-1} and 1.9×10^{-4} S cm^{-1}, respectively. The electrochemical profile of the cell is depicted in Fig. 4 d. The battery was tested at C/40, C/10, and C/2 current rates over 0 and 2.2 V voltage window and at 200 °C. Upon the first charge at C/40 rate, excessive capacity (+25% of the theoretical capacity) was obtained which wasn't understood by the authors. Moreover, 85% of the theoretical capacity was reversible at C/10 and about 50%–25% at C/2. The low capacities obtained when increasing the current rate is because of to the ionic and electronic kinetic limitations and the observed cracks within the particles occurring because of volume change during the Na-insertion and extraction. NASICON $Na_{3+x}Sc_2Si_xP_{3-x}O_{12}$ (where $0.05 \leq x \leq 0.8$) were first investigated by Guin et al. [35] as solid electrolytes. Solid-state was chosen as synthesis method using $NH_4H_2PO_4$, Sc_2O_3, Na_2CO_3, and SiO_2 precursors. Several thermal treatments and intermediate grindings were carried out to obtain the targeted phase. This study provided valuable understandings on the substitution effect of P with Si on the sodium ion conductivity where it reaches its maximum value of 6.9×10^{-4} S cm^{-1} at 25 °C for x = 0.4. Passerini's group [36] worked on developing a hybrid Na-conducting solid electrolyte via coating $Na_3Si_2Y_{0.16}Zr_{1.84}PO_{12}$ N-butyl-N-methylpyrrolidinium bis(trifluoromethanesulfonyl)imide ionic liquid (abbreviated as Py14TFSI). The preparation was performed inside an Argon-filled glove box. The NASICON powder and Py14TFSI were dissolved in acetonitrile and left under magnetic stirring overnight. Later, the solvent was evaporated at 70 °C and the resulting powder was further dried under vacuum at 120 °C. For comparison, Py14TFSI mixed with NaTFSI salt were used as well. The electrical characterization carried on the hybrid electrolyte demonstrated slower ion transport properties. No significant enhancement of the Na^+ mobility at the NASICON grain-grain interface was noticed after its coating with Py14TFSI ionic liquid. In 2011, $Na_2M_2TeO_6$ (M = Ni, Co, Zn, Mg) were first studied by Kataev et al. [37] as a new layered sodium oxide. In 2018, Li et al. [38] worked on Ga-substituted $Na_{2-x}Zn_{2-x}Ga_xTeO_6$ (x = 0, 0.05, 0.1, 0.15) as inorganic solid electrolyte. The composition with x = 0.1 exhibits the best IC around 1.1×10^{-3} S cm^{-1} at RT compared to only 0.6×10^{-3} S cm^{-1} for $Na_2Zn_2TeO_6$. This oxide was tested using $Na_3V_2(PO_4)_3$/-$Na_{1.9}Zn_{1.9}Ga_{0.1}TeO_6$/Na configuration cell. At 80 °C and 0.2C current rate, a reversible specific capacity of 70 mAh g^{-1} for 10 cycles was obtained. Perovskites [39–41] were studied as well as qualified inorganic SSE materials. For example, Zhao et al. [39] studied a novel perovskite-type $Na_{1/3}La_{1/3}Sr_{1/3}ZrO_3$ in 2019, synthesized using a solid-state reaction at 1300 °C. Stoichiometric amounts of Na_2CO_3, La_2O_3, $SrCO_3$, and ZrO_2 were used as raw materials with 10 wt% excess of Na. $Na_{1/3}La_{1/3}Sr_{1/3}ZrO_3$ demonstrates a high IC of 1.025×10^{-5} S cm^{-1} at 25 °C due to the beneficial effect of Sr doping where the SSE is densified after sintering.

2.2. Organic solid electrolytes

Gel polymer electrolytes (GPE) consists of hybrid structure combining polymer and liquid electrolyte. Therefore, GPE hold the privilege of merging both mechanical properties of solids and diffusive properties of liquids. They show high IC, large electrochemical stability window, better compatibility with the electrode materials and high thermal stability [42].

Yang et al. [42] investigated a new GPE based on poly(vinylidene difluoride-co-hexafluoropropylene) (abbreviated as P(VDF-HFP)). The choice of this polymer was made based on its interesting properties. It shows a high electrochemical stability thanks to the strong electron-withdrawing functional group (–C–F). P(VDFHFP), is a semi-crystalline polymer revealing high flexibility and a dielectric constant (~8.4) enabling fast lithium salt dissolution and high concentration of charge carriers. The synthesis of the GPE based on P(VDF-HFP) was carried out by following a simple separation process. At the beginning, 15 wt% of P(VDF-HFP) is dissolved in 3 wt% distilled water and 85 wt% N,N-dimethyl formamide (DMF), the mixture is casted in a glass plate and immersed in water at 80 °C in order to obtain a homogeneous film. Later, vacuum drying of the sample at 100 °C for 10 h time is necessary before transferring it to a glove box. Then, to succeed the preparation of the GPE, the dried sample is immersed this time in an organic electrolyte (1 M $NaClO_4$ dissolved in Ethylene Carbonate (EC): Dimethyl Carbonate (DMC): Ethyl Methyl Carbonate (EMC)) for 12 h. A

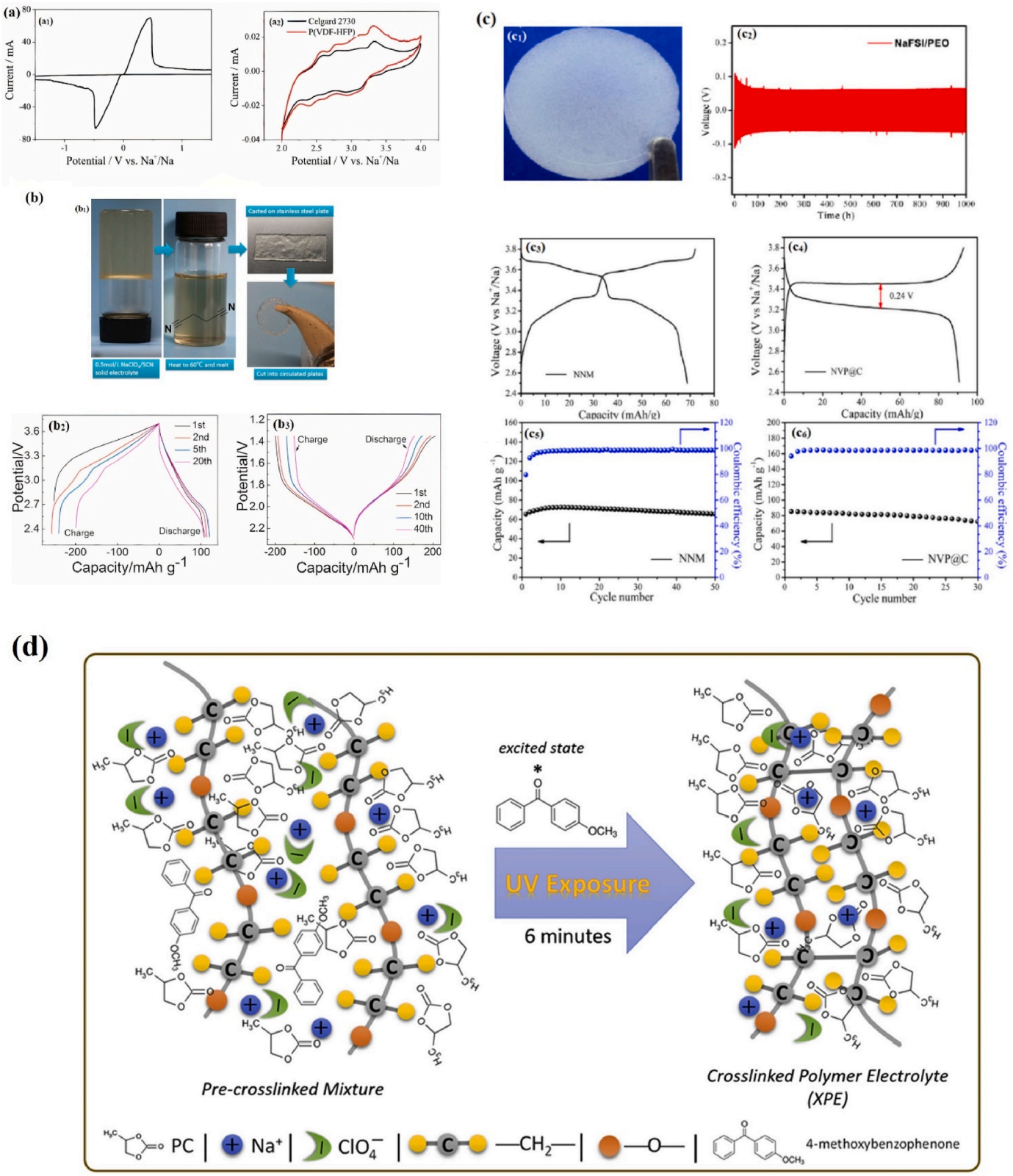

Fig. 5. CV curve at RT of **(a_1)** Na/GPE/Na with 1 mV s^{-1} scan rate, **(a_2)** $Na_4Mn_9O_{18}$/GPE/Na and $Na_4Mn_9O_{18}$/Celgard 2730/Na at 0.1 mV s^{-1} scan rate [42] (Copyright 2015, Elsevier). **(b)** Synthesis steps of Na–SCN PCEs (b_1), Potential vs. capacity profile of P(AN-NA) cathode (b_2), PAQS anode (b_3) at 50 mA g^{-1} with 5 mol % $NaClO_4$–SCN PCE [44] (Copyright 2015, Elsevier). **(c_1)** Picture of the as-prepared membrane of SPE, **(c_2)** Cycling performance for the Na|Na symmetric cells with NaFSI/PEO electrolyte at 0.1 mA cm^{-2} and 80 °C, voltage vs. capacity profile of **(c_3)** NNM and **(c_4)** NVP@C in SPE-based cells, Capacity vs. cycle number of NNM **(c_5)** and NVP@C **(c_6)** [63] (Copyright 2016, Wiley). **(d)** Schematic illustration of XPE preparation [64] (Copyright 2017, Elsevier).

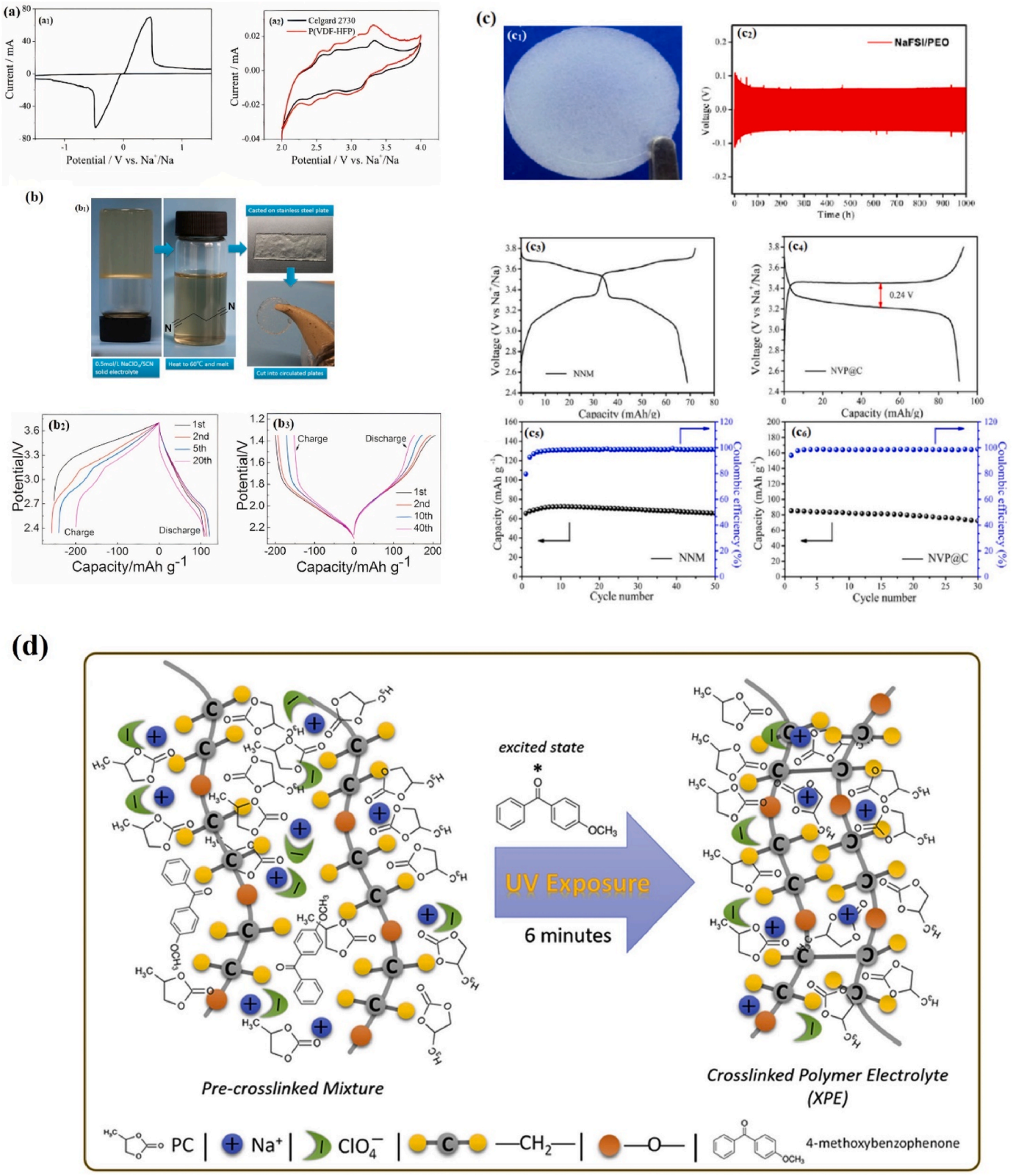

Fig. 5. (*continued*).

cyclic voltammetry (CV) test was performed on SS/GPE/SS (SS: stainless steel, blank test) and Na/GPE/Na cells to evaluate the Na^+ ion conduction. Reversible redox peaks at 0.5 and 0.5 V (vs. Na^+/Na) were detected, as shown in Fig. 5 a_1, confirming the deposition and dissolution of sodium, respectively. Whereas no peaks were observed for the blank test. The sodium IC of P(VDF-HFP) GPE at RT is 0.60 mS cm ^{1}, superior to that of Celgard 2730 which is only equal to 0.16 mS cm ^{1}. Furthermore, the ionic transference number of sodium ion (t_{Na}^{+}) shown by the prepared GPE is 0.30, superior to that of Celgard 2730 (~0.17). The performance of the P(VDF-HFP) GPE was tested using $Na_4Mn_9O_{18}$

and metallic Na as the positive and negative electrode materials and compared to that of Celgard 2730. As shown in Fig. 5 a_2, the cyclic voltammetry curves demonstrate the reversibility of the redox reaction where five peaks were detected in each of the anodic and cathodic scans. The area of the peaks is higher for P(VDF-HFP) which proves better redox kinetics, and these results are in good agreement with the superior IC and t_{Na}^{+} shown by the GPE.

In 2018, Guo et al. [43] studied a GPE based on poly (vinylidenefluoride-cohexafluoropropylene), denoted as P(VDF-HFP) and tested it in an electrochemical cell using $Na_3V_2(PO_4)_2O_2F$ as cathode and hard carbon issued from cotton cloth as anode. Its preparation consisted of dissolving P(VDF-HFP) polymer in N,N-dimethyl formamide (DMF) and distilled water (17:1, weight ratio), then heated at 80 °C before casting the resulting mixture on a watch-glass. A white homogeneous film was obtained after solvents evaporation and followed by vacuum drying at 100 °C. Afterwards, the film was soaked in 1 M $NaClO_4$ dissolved in 95 wt% propylene carbonate and 5 wt% fluorinated ethylene. The prepared gel electrolyte was tested in half-cells and in full cell as well. In $Na_3V_2(PO_4)_2O_2F$/Na half-cell, a capacity of 120 mAh g^{-1} was obtained for 1500 cycles at 1C current rate. In a full cell configuration, a reversible capacity of 120 mAh g^{-1} and 80 mAh g^{-1} for 200 cycles were delivered at 1C and 10C-rates, respectively.

Plastic crystal electrolytes (PCEs) are considered as new type of SEEs. They are prepared by the dissolution of ionic salts in a polar molecular solid and they exhibit rather high IC. Zhu et al. [44] reported PCE based on succinonitrile (NRC–CH_2–CH_2-CRN, denoted as SCN) as a solid solvent and doped Na^+ salts into the organic solid matrix. The preparation process is performed in argon atmosphere where 0.5% mol $NaClO_4$ salt is dissolved in melted SCN at 60 °C for 24 h. The mixture is casted on a stainless steel to form a uniform transparent film after slow cooling (Fig. 5 b_1). The prepared $NaClO_4$–SCN-PCE shows a high IC of 10^{-3} S cm^{-1} at RT and works in a voltage window above 3 V. The electrochemical performance of the solid electrolyte was studied in an all-organic sodium-ion battery. Fig. 5 b_2 shows the potential vs. capacity profile of the half-cells poly(aniline/o-nitroaniline) (denoted as P (AN-NA) vs. Na^+/Na and poly(anthraquinonyl sulfide) (denoted as PAQS) vs. Na^+/Na. The P(AN-NA) cathode delivers a reversible capacity of 120 mAh g^{-1} with a sloping discharge plateau from 3.7 V to 2.3 V and a capacity retention of 94% after 20 cycles. Furthermore, the PAQS anode shows a high discharge capacity around 205 mAh g^{-1} with a plateau at 1.9 V and a capacity retention of 75% after 40 cycles (Fig. 5 b_3).

Solid polymer electrolytes (SPEs) are prepared by the dissolving Na-salts in ion-coordinating macromolecules. SPEs demonstrate good flame resistance and high flexibility in comparison to organic liquid electrolytes. High temperature is necessary to obtain sufficient IC. For instance, polyethylene oxide (PEO) based SPEs require working temperature of 60 °C for their application in LIBs. However, the melting temperature of sodium is 98 °C which rises challenges for the use of SPEs in SIBs [45, 46]. Many polymers were studied for the preparation of SPEs such as polyvinyl alcohol (PVA) [47–51], polyacrylonitrile (PAN) [52–54], and poly-(vinyl pyrrolidone) (PVP) [55–59], poly(methyl acrylate) (PMA) [60–62], and poly(ethylene glycol) (PEG) [45,46,60].

Qi et al. [63] studied a SPE considering sodium bis(fluorosulfonyl) imide (NaFSI) as salt and PEO as polymer (EO: $Na^+ = 20$, by molar ratio) exhibiting superior IC of 4.1×10^{-4} S cm^{-1} at 80 °C. The prepared electrolyte (Fig. 5 c_1) was tested in half-cells against Na metal using $Na_{0.67}Ni_{0.33}Mn_{0.67}O_2$ and $Na_3V_2(PO_4)_3$@C cathodes. As revealed in Fig. 5 c_2, a stable interface between the SSE and the cathode materials was achieved which goes in total agreement with the obtained data for the tests conducted on Na | Na symmetric cells with NaFSI/PEO electrolyte A current density of 0.1 mA cm^{-2} was applied to the cell and the voltage of sodium deposition/dissolution was recorded revealing that the polarization decreases at the beginning and then stabilizes at around 60 mV for a time over than 1000 h. Therefore, the solid electrolyte interphase (SEI) is stable after its formation in the first cycles. At 0.2C current rate and 80 °C, the solid polymer electrolyte performs well as shown by the electrochemical tests reported in Fig. 5 c_3-c_6. Capacities of 60 mAh g^{-1} and 80 mAh g^{-1} were delivered for $Na_{0.67}Ni_{0.33}Mn_{0.67}O_2$ (NNM) and $Na_3V_2(PO_4)_3$@C (NVP), respectively. Colò et al. [64] developed a rapid, solvent-free, and scalable preparation route for the synthesis of PEO-based SSE. To this end, a light-induced free-radical polymerization (UV curing) method was chosen. $NaClO_4$, PC, PEO precursors following the weight ratios 5, 50, 45, respectively, were mixed with 4 wt% of photo-initiator to form a viscous gel and cast it to form an uniform film. Later, the film was irradiated using UV light with 30 mW cm^{-2} intensity for 3 min. The preparations were carried in an environmentally controlled dry room (relative humidity <2% ± 1 at 20 °C). Furthermore, the crosslinked PEO-based polymer electrolyte (denoted as XPE) was obtained with curing under nitrogen atmosphere and at ambient temperature (Fig. 5d). At 25 °C, the IC of XPE is around 1 mS cm^{-1} and stable at 4.7 vs. Na^+/Na voltage. XPE was tested in TiO_2/X-PE/Na cell delivering a capacity of 250 mAh g^{-1} and 200 mAh g^{-1} at ambient temperature with 0.1C and 0.2C current rates. Du et al. [5] studied the high efficiency of perfluorinated sulfonic (PFSA-Na) SPE in a wide range of temperature from −35 °C to 25 °C. For its preparation, the authors started by dissolving PFSA-Na in N, N-dimethylformamide (DMF) solvent and leaving it stir overnight and then, 1 M NaClO4 in EC: DEC was added and left again stir for 12 h time. The resulting solution was coated and dried to obtain PFSA-Na membranes. The IC of PFSA-Na is measured around 2.85×10^{-6} S cm^{-1} at −35 °C. The efficiency of the polymer solid electrolyte was tested using half-cell Na||$Na_4Fe(CN)_6$ demonstrating only 0.014% capacity fade per cycle for 1100 cycles and at 1C current rate. Moreover, PFSA-Na membranes have shown 100% coulombic efficiency (CE) at different temperatures.

Chen et al. [65] first investigated a plastic crystal SPE with anion-trapping boron moieties (B-PCPE). The latter was synthesized via in situ growth using UV-curing technique. The prepared B-PCPE shows good IC of 0.36 mS cm^{-1} at 25 °C and t_{Na}^{+} of 0.62. The electrochemical efficiency of B-PCPE was studied in a full cell configuration with $NaNi_{1/3}Fe_{1/3}Mn_{1/3}O_2$ as cathode and hard carbon as anode. At 0.1C-rate, a capacity of 104.8 mA h g^{-1} was delivered with 80% capacity retention for 120 cycles. UV-curing technique enhances ion transport through the electrode/electrolyte interface. In 2020, Gao et al. [66] reported the use of perfluorinated sulfonic resin PFSA-Na as PSE for all-solid-state SIBs. The IC of PFSA-Na is around 3.35×10^{-3} S cm^{-1} and 8.7×10^{-4} S cm^{-1} at 55 °C and −25 °C, respectively. The cell $Na_2TiV(PO_4)_3$@C/PFSA-Na/Na exhibits a stable capacity of 100 mAh g^{-1} for

Table 1
Examples of SPEs formulations from literature, their IC, and E_a.

Formulation	IC (S cm^{-1})	E_a (eV)	Reference
PEO-$NaClO_4$ (EO/Na^+: 12/1, molar ratio)	3.1×10^{-6} at 60 °C		[67]
PEO-$NaPF_6$ (EO/Na^+ = 0.065, molar ratio)	5×10^{-6} at 25 °C		[68]
PEO: PEG: $NaClO_3$ (30: 60: 10, molar ratio)	3.40×10^{-6}	0.417	[69]
NaTFSI-$(PEO)_n$ (n = 9)	4.5×10^{-5} at 20 °C		[70]
PEO: NaClO4	1.34×10^{-5} at 60 °C		[71]
5 wt%TiO2: PEO: NaClO4 (EO/Na^+ = 20, molar ratio)	2.62×10^{-4} at 60 °C		[71]
PEO: $NaClO_4$: Na-CMC (82: 9: 9, molar ratio)			[72]
PVA/NaBr (7:3, weight ratio)	1.362×10^{-5} at 40 °C	0.326	[73]
PAN + 24 wt% $NaCF_3SO_3$	0.71×10^{-3}	0.23	[74]
PVP/$NaClO_3$ (7: 3)		0.26	[75]
PEO/PVP with 15 wt% NaF			[76]
PMA/PEG hybrid polymer with 5% nano-α-Al_2O_3	1.46×10^{-4} at 70 °C		[60]

300 cycles for 100 mA g ^{1} current density.

Table 1 presents some examples from literature of SPEs, their IC, and E_a.

2.3. Hybrid solid electrolytes

Ni'maha et al. [71] emphasized the use of a new SPE nanocomposite electrolyte (denoted as nCPE) based on polyethylene glycol (PEO), $NaClO_4$ and titanium dioxide. Two electrolytes PEO/$NaClO_4$ and TiO_2/PEO/$NaClO_4$ were prepared for the sake of comparison using solution casting method. The first SSE was formulated using different PEO and $NaClO_4$ ratios by dissolving them in anhydrous acetonitrile until homogenization, then casted in a Teflon plate and left to dry at 55 °C for 6 h. For the second electrolyte, $TiCl_4$, deionized water, urea and ethanol were mixed and left under magnetic stirring for 15 min at less than 5 °C. Solution of PEO in ethanol was added to the first solution and stirred together for 15 min. Later, the Teflon container was transferred to an autoclave and heated at 200 °C for 2 h. The final product was recovered by centrifugation and left to dry under vacuum overnight. Fig. 6a and b shows a photograph of both solid polymer electrolyte films. The IC measurements reveal that the addition of 5 wt% TiO2 enhanced it to a maximum of 2.62.10 ^{4} S cm ^{1} at 60 °C. The electrochemical efficiency of the prepared TiO2/PEO/NaClO4 nCPE was tested using $Na_{2/3}Co_{2/3}Mn_{1/3}O_2$ cathode versus metallic Na and compared to the 1 M $NaPF_6$ in EC: PC (Fig. 6c). The SSE demonstrates good stability for 25 cycles with a capacity of 45 mAh g ^{1} which represents around 45% of the reversible capacity obtained using liquid electrolyte.

In 2018, Zhang et al. [60] prepared a composite polymer electrolyte (CPE) based on PMA and PEG. These authors used the following preparation protocol: azodiisobutyronitrile and PEG were stirred and then, methacrylate solution was added and left at 70 °C. Later, nano-α-Al_2O_3 dissolved in acetone and 0.6 M $NaClO_4$ were added as well and left under magnetic stirring for 1 h before casting it in a Teflon substrate and drying it to form a film. The as-synthesized solid electrolyte demonstrates high IC of 1.46 × 10 ^{4} S cm ^{1} at 70 °C, good mechanical

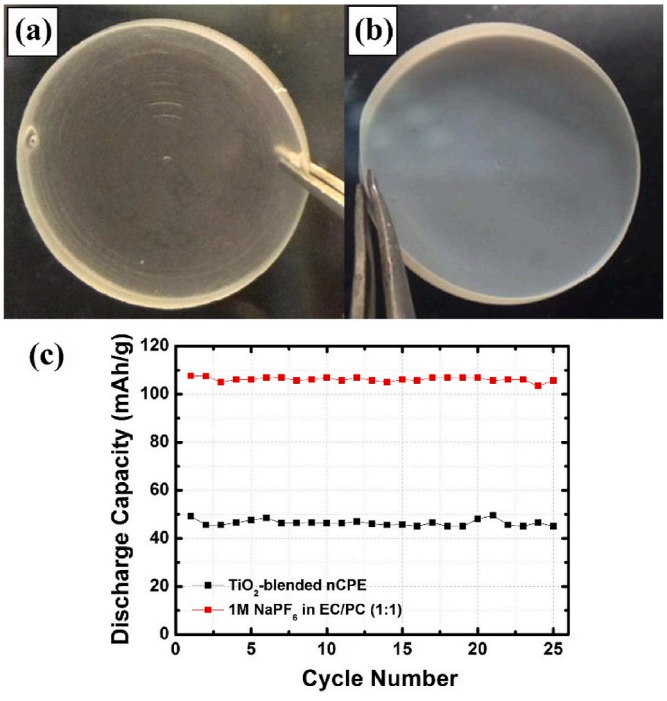

Fig. 6. Photographs of PEO/$NaClO_4$ SPE membrane, **(a)** EO:Na 20, and **(b)** 5% TiO_2-blended nCPE (EO:Na 20), **(c)** Discharge capacity vs. cycle number of $Na_{2/3}Co_{2/3}Mn_{1/3}O_2$//Na half-cell at 0.1 C-rate using SPE and liquid electrolyte [71] (Copyright 2015, Elsevier).

properties (Young's modulus is around 50.79 MPa), and it is electrochemically stable to 4.5 V vs. Na^+/Na. The composite electrolyte PMA/PEG hybrid polymer with 5% nano-α-Al_2O_3 was tested using Na metal as counter electrode and $Na_3V_2(PO_4)_3$ as cathode. At 70 °C and 0.5C-rate, a capacity of 85 mAh g ^{1} for 350 cycles was maintained. The combination of PEG, PMA, and nano-α-Al_2O_3 was selected to ensure good contact between the solid electrolyte and the electrode where PEG serves for Na $^{+}$ ions transmission, PMA is a film-forming agent and contributes to the dissociation of $NaClO_4$ thanks to the carbonyl group which demonstrate strong polarity, while nano-α-Al_2O_3 here is an inorganic filler which reduces the crystallinity.

In 2019, Xie et al. [25] synthesized a quasi-SSEs (denoted QSSE) based on poly(vinylidene fluoride-co-hexafluoropropylene) (PVDF-HFP) cross-linked with Al_2O_3 nanoparticles. PVDF-HFP was first dissolved in ethanol: acetone mixture (1:5 vol ratio) and heated at 60 °C for 1 h. Later, Al_2O_3 nanoparticles using different ratios were added and left stir for 2 h at the same temperature. The resulting white gel is casted on a glass plate and dried under vacuum at 70 °C for 12 h. Afterwards, the obtained film was cut into disks, transferred to the glovebox, and soaked for 2 h in 1 M $NaPF_6$ in EC: DMC: EMC (1:1:1, by volume). This GPE demonstrates high IC up to 1.3 × 10 ^{3} S cm ^{1}. In cell configuration of Graphite||QSSE||Sn, a stable capacity of 96 mAh g ^{1} was delivered at 5C-rate with 97% retention for 600 cycles.

Cheng et al. [77] worked on the elaboration of a hybrid solid electrolyte (H-SSE) from poly PVDF-HFP polymer and $Na_3Zr_2Si_2PO_{12}$. For its preparation, the three reagents 90 wt% PVDF-HFP, 10 wt% $Na_3Zr_2Si_2PO_{12}$ and PEG (95: 5 wt ratios of PVDF-HFP and NASICON to PEG) were ball-milled in N, N-dimethylacetamide (DMF) and acetone (1:2) solvents for 30 h at 300 rpm. By the end, the mixture was casted on a glass plate and then, the solvents were evaporated. Later, the obtained film was immersed in deionized water for 30 min, dried first at 60 °C for 12 h, and second under vacuum at 70 °C for 6 h. The solid membrane was pressed at 2.5 MPa and then, soaked in 1 M $NaClO_4$ in EC: DMC for 3 min and then pressed at 5.0 KPa to expel the excess of liquid electrolyte. To enhance the formation of a film, PEG was added to the formulation. The H-SSE shows a high IC around 2.25 × 10 ^{3} S cm ^{1} at RT. In a half-cell configuration of $Na_3V_2(PO_4)_3$/C vs. metallic sodium, a capacity of 90 mAh g ^{1} at 0.5C was delivered for 175 cycles. Another study reported by Chen et al. [78] in August 2020 has emphasized the use of hyperbranched polyether-based electrolytes for all-solid-state SIBs. They show a high IC of around 5.7 × 10 ^{4} S cm ^{1} at 27 °C, in comparison to the linear polyether-based electrolyte where its IC is inferior to 10 ^{5} S cm ^{1} at 25 °C. However, the obtained membrane is fragile and therefore, adding poly(vinylidene fluoride) hexafluoro propylene polymer is fundamental to reinforce it.

Gao et al. [2] conducted a new strategy to develop an ionogel electrolyte for QSSEs SIBs based on NaTFSI salt and N-propyl-N-methylpyrrolidinium bis-(fluorosulfonyl)imide (denoted as PY13FSI). The preparation of Na-based ionic liquid (abbreviated as Na-IL) electrolyte consists of dissolving first the Na-salt in PY13FSI. Then, SBA-15 (SiO_2-2D mesoporous molecular Sieve) was added to the mixture and ball-milled for 12 h at 400 rpm speed. Afterwards, PVDF HFP was added to enhance the mechanical properties. The ratio of Na-IL and PVDF HFP was optimized to 2.7/0.2 and demonstrated superior IC of 2.48 × 10 ^{3} S cm ^{1} at 30 °C and t_{Na}^{+} of 0.37. The prepared electrolyte was tested using $Na_3V_2(PO_4)_3$ as cathode and Na as counter-electrode. At 0.1C rate, a capacity of around 100 mAh g ^{1} was delivered for 300 cycles. Ball-milling has reduced the size of SBA-15 which positively impacted the properties of the resulting electrolyte. Hydrogen bonds with FSI , TFSI , and Si–OH were formed which facilitated the dissociation of NaTFSI and increase Na^+ ions migration. Table 2 summarizes a comparison between different SSEs, their physico-chemical and electrochemical properties.

Table 2
Comparison between different SSEs, their physico-chemical and electrochemical properties.

Solid electrolyte type	Composition	Synthesis Method	IC(S cm ^{1})	E_a for conduction of (kJ mol ^{1})	Positive electrode	Negative electrode	Voltage range (V)	Electrochemical properties	Ref
Inorganic	Na_3PS_4 glass	Mechanochemical technique	6 × 10 ^{6} at 25 °C	47	TiS_2	Na–Sn alloy		90 mAh/g for 10 cycle at 25 °C and 25 °C at 0.013 mA cm ^{2}	[34]
Inorganic	$Na_3Zr_2Si_2PO_{12}$	Sol-gel	1.5 × 10 ^{3} at 200 °C		$Na_3V_2(PO_4)_3$	$Na_3V_2(PO_4)_3$	0–2.2	1.04 mA h (C/10 at 200 °C)	[34]
Inorganic	Na_3PS_4	Mechanoch-emical technique	4.6 × 10 ^{6}		TiS_2	Na–Sn alloy			[28]
Inorganic	Na_3PS_4 glass-ceramic	Mechanochemical technique	4.6 × 10 ^{6}		$NaCrO_2$	$Na_{15}Sn_4$	1.2–4.0	60 mAh/g at 0.13 mA cm ^{2} for 30 cycle	[42]
Gel polymer	Poly(vinylidene difluoride-co-hexafluoropropylene) (P(VDF-HFP)	Phase separation process	0.60 × 10 ^{3} at 25 °C	4.6	$Na_4Mn_9O_{18}$	Na metal	2.0–4.0		[42]
Organic - Plastic Crystal Electrolyte (PCE)	$NaClO_4$-Succinonitrile (NRC–CH_2–CH_2-CRN, SCN)	Wet chemistry	~10 ^{3} at 25 °C		Poly(aniline/o-nitroaniline) (P(AN-NA))	Poly (anthraquinonyl sulfide) (PAQS)	1.3–4.9	**P(AN-NA):** 113 mAh/g at 50 mA/g for 20 cycle **PAQS:** 205 mAh/g at 50 mA/g with capacity retention of 75% after 40 cycles	[44]
Nanocomposite Polymer	TiO_2/PEO/$NaClO_4$	Solution casting technique	2.62 × 10 ^{4} at 60 °C		$Na_{2/3}Co_{2/3}Mn_{1/3}O_2$	Na metal	1.25–4.3		[4, 56]
Inorganic	$Na_{3+x}Sc_2Si_xP_{3-x}O_{12}$	Solid state	6.9 × 10 ^{4} at 25 °C						[35]
Inorganic	Na_3PS_4 Na-β''-Al_2O_3	Solid state	0.04 × 10 ^{3} at 25 °C 2.1 × 10 ^{3} at 25 °C						[29]
Inorganic	Na_3SbS_4	Solution-processing Solid state	1.1 × 10 ^{3} at 25 °C	0.20 eV	Na_3SbS_4-coated $NaCrO_2$			110 mAh/g at 50 mAcm ^{2} and 30 °C	[32]
Inorganic	Cl-doped Na_3SbS_4	Solid state	1.14 × 10 ^{3} at 303 K	249 eV	TiS_2	Na metal	1.2–2.4	80 mAh g ^{1} at C/10 over 10 cycles at RT	[23]
Solid Polymer electrolyte	Sodium Bis (fluorosulfonyl)imide/ Poly(ethylene oxide) NaTFSI-PEO		4.1 × 10 ^{3} at 80 °C						[63]

3. Solid-state electrolytes for potassium-ion batteries

In 2004, A. Eftekhari [79] introduced the concept of KIB by using Prussian blue cathode. This KIB model has exhibited a cycling performance of 500 cycles with a capacity retention of 88%. Subsequently, Prussian blue materials and their analogues (PBAs) have gotten considerable attraction as cathode materials for both SIBs and LIBs technologies. A year later in 2005, a patent was filed on the upcoming electrolyte potassium hexafluorophosphate (KPF_6) for KIBs [80]. Later, research on KIBs has been stagnated for many years owing to the safety concerns related with the potassium and the increasing attractiveness of LIBs and SIBs technologies due to their superior performance. Ten years later, a significantly increasing number of scientific publications can be evidenced since 2015 owing to the reversible K-insertion into graphite investigated by Komaba et al. [81] that has reinforced the interest of graphitic materials as anodes in KIBs. In recent years, further potential electrode materials have been successfully investigated for KIBs, which can be obviously observed through the increasing number of publications. All these accomplishments are greatly pushing forward the progress of KIBs.

Although huge improvement has been made since 2015, there are still existing many challenges, especially the severe side reaction between electrolyte and potassium metal due to its great reactivity, which leads to an unstable SEI and low CE [82]. Hence, an outstanding electrolyte might be the crucial part for the development of KIBs. Unfortunately, no methodical research has been accomplished to investigate the electrolyte and its effect on the performance yet while considering safety issues. To compensate for this limitation, SSEs have attracted more interest as they are non-flammable and present no consequence of leakage nor explosion [83]. SSEs are commonly categorized as inorganic, organic, and hybrid [84]. While the high IC of inorganic-based SSEs has showed much interest, the hard synthesis conditions (high temperature) and weak interface contact with electrodes which largely obstruct its further improvement. Compared to this type, organic-based electrolytes are facile to synthesize, chemically stable and show excellent contact interface with the electrodes [83]. Nevertheless, the low IC of organic-based electrolytes at RT limits their use, especially at low operating temperatures. Therefore, the hybrid-based type could be a great alternative, combining the properties of all the above SSE types.

The trend of using SSEs for KIBs started in 2018, through an investigation of inorganic $K_2Fe_4O_7$, prepared by a hydrothermal reaction. The three-dimensional open framework $K_2Fe_4O_7$ demonstrates high ionic

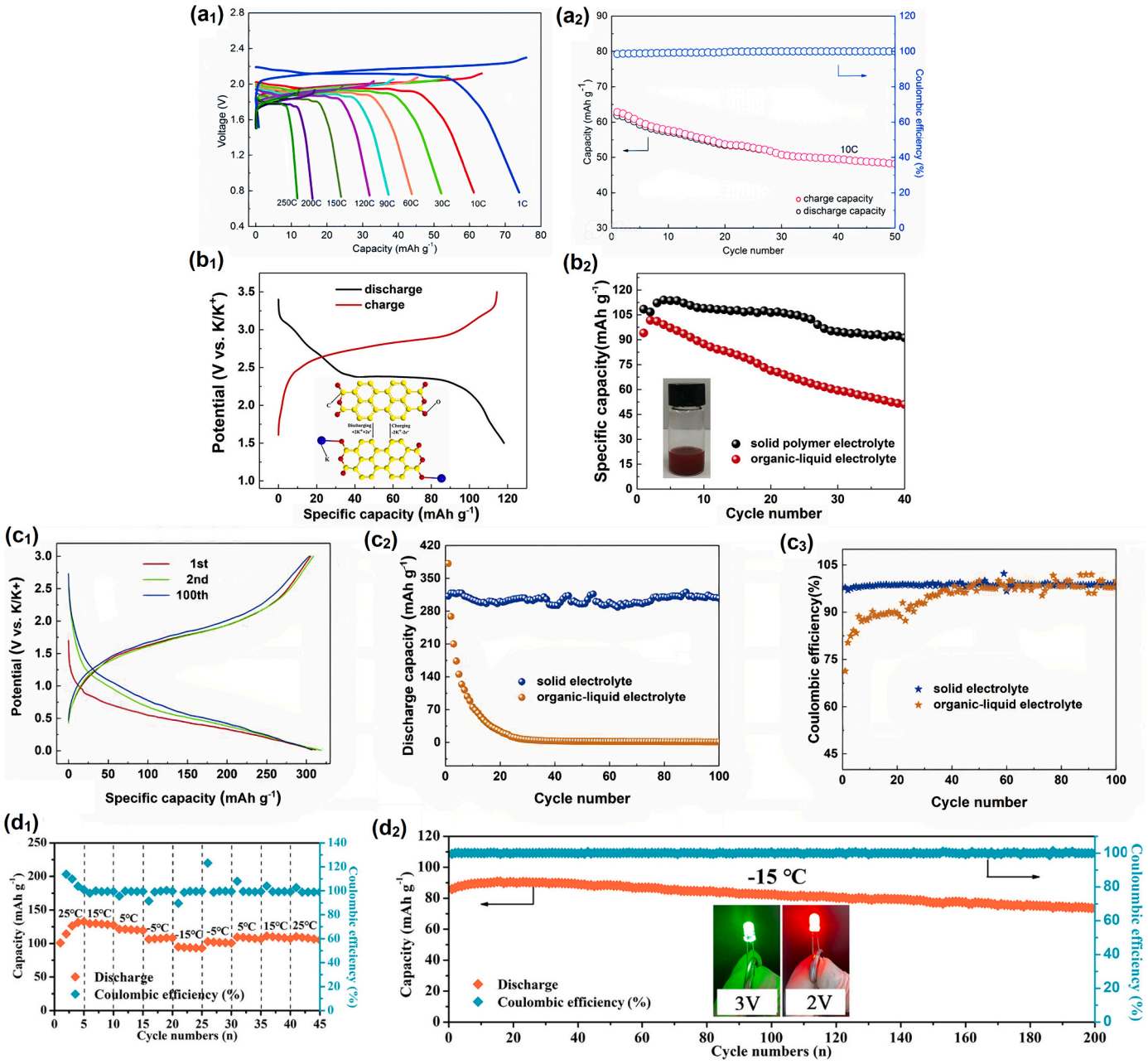

Fig. 7. **(a_1)** Voltage vs. capacity profile at different C-rates, **(a_2)** capacity vs. cycle number all-SSB ($KFe_2(CN)_6$, xH_2O ||$K_2Fe_4O_7$ || $KFe_2(CN)_6$, xH_2O) at 10C [89] (Copyright 2018, RSC). **(b_1)** Voltage vs. capacity profile of PTCDA || PPCB-SPE ||K metal cell at 10 mA g^{-1}, **(b_2)** capacity vs. cycle number of PTCDA with PPCB-SPE or organic-liquid electrolyte at 20 mA g^{-1} [86] (Copyright 2018, Elsevier). **(c_1)** Voltage vs. capacity profile 25 mAh g^{-1} of the SSBs with PEO-based SPE, **(c_2)** Capacity vs. cycle number at 25 mA g^{-1} and **(c_3)** CE of 3 h Ni_3S_2@Ni with PEO-based SPE or the organic-liquid electrolyte [87] (Copyright 2019, Elsevier). **(d_1)** Rate capability and **(d_2)** capacity vs. cycle number of PCTDA || PFSA-K || Graphite full cell at −15 °C [83] (Copyright 2021, Elsevier).

mobility (IC = 5 × 10 ^{2} S cm ^{1} at RT and E_a = 0.08 eV). As shown in Fig. 7 a_1, the all-SSB with Prussian blue analogue cathode exhibits a capacity of 13 mAh g ^{1} and 87 mAh g ^{1} at 250C and 1C, respectively. The rate capability is outstanding compared to those of KIBs using liquid electrolytes, where metallic potassium is highly reactive using liquid electrolytes, and the compared to the reported performances for all-SSBs in LIBs and SIBs [85]. Moreover, capacity retention of 78% CE of about 100% were obtained after 50 cycles at 1C-rate (Fig. 7 a_2). Fei et al. [86] studied for the first time an SSB KIBs with 3,4,9,10-perylene-tetracarboxylicacid dianhydride (PTCDA) as positive electrode and hybrid SPE. Poly(propylene carbonate) (PPC)–KFSI mixed with cellulose nonwoven backbone SPE (PPCB-SPE) shows an IC of 1.36 × 10 ^{5} S cm ^{1} at 20 °C. Moreover, PTCDA in all-SSBs demonstrates a working voltage of 2.3 V, a high first capacity of 118 mAh g ^{1} at 10 mA g ^{1}, an energy density 271 Wh kg ^{1}, and a stable cycling performance, as demonstrated in Fig. 7 b_1. After 40 cycles, the cell retains 84% of its initial capacity. Also, it still provides a capacity of 91.17 mA g ^{1}, in contrast the cell with non-aqueous liquid electrolyte suffered from a great capacity fading of 45.7%. This capacity loss might be resulted from the high solubility of PTCDA into the organic-liquid electrolyte as shown in Fig. 7 b_2, revealing the crucial interest of the use of SSEs in the case of organic electrodes paving the way for further investigations. One year later, the same group designed Ni_3S_2@Ni electrode for KIBs with poly(ethylene oxide)-bis(flourosulfonyl)imide (PEO-KFSI)-based hybrid electrolyte [87]. The IC of PEO-KFSI reaches up to 2.7 10 ^{4} S cm ^{1} at 60 °C. Regarding the electrochemical performance, the first reversible capacity

provides 312 mAh g ^{1}, as well as a high CE of 97%. The high CE may be assigned to the small SEI layer. In addition, the initial CE is much higher than that reported for transition metal sulphides using organic-liquid electrolytes in KIBs (Fig. 7 b_3). In the following cycles, the long-term cycling shows no capacity loss, even after 100 cycles, as shown in Fig. 7 c_1. The capacity retention and CE of both solid and liquid state KIBs were conducted at a current density of 25 mA g ^{1}. As revealed in Fig. 7 c_2, the initial reversible capacity of KIBs with organic-liquid electrolyte is 381 mAh g ^{1}, which is superior to the one reported using SSE (312 mAh g ^{1}). However, the cell with liquid electrolyte displays a huge capacity decay, and low capacity of only 24 mAh g ^{1} after 20 cycles. As aforementioned, the large capacity loss during the electrochemical cycling were attributed to the high solubility of polysulphides into organic solvents. Furthermore, polysulphides might also react with carbonate-based electrolyte, resulting in cell failure [88]. On contrary, the cell with PEO-KFSI based-hybrid electrolyte shows good reversible capacity of 307 mAh g ^{1} after 100 cycles, denoting that hybrid electrolyte ensures safety and limits capacity decay during the electrochemical cycling [87].

In 2021, Guangyuan Du et al. [83] developed simple preparation process of hybrid electrolyte membranes using perfluorinated sulfonic resin (PFSA-K) for low-operating temperature use. The PFSA-K membranes display advantageous ionic mobility of potassium at a large temperature range from 15 to 85 °C, good electrochemical performances, and high mechanical properties. Furthermore, PTCDA as cathode and graphite as anode, were chosen for the electrochemical tests. The synthesized hybrid electrolyte exhibits good mechanical flexibility, excellent electrochemical stability, and high IC of 9.3 × 10 ^{5} S cm ^{1} at RT. Furthermore, the full cell (Fig. 7 d_1) displays reversible capacity of 95 mAh g ^{1} even at a low temperature of 15 °C. When increasing the temperature to 25 °C, the reversible capacity was retained. Fig. 7 d_2 shows capacity retention exceeding 85% after 200 cycles at 15 °C and 100 mA g ^{1}. It was also noticed (Fig. 7 d_2) that the obtained CE was around 100%, which means that the PFSA-K membrane is stable, and can be used in low-operating temperature.

Based on the above discussion, we have summarized several kinds of methods to enhance the performance of SSEs for KIBs, including the design of SSEs, selection of appropriate electrodes, and type of SSEs. Furthermore, we also listed the important parameters including cycling stability, rate capability, IC, cell configuration, E_a, flexibility and electrolyte of recent work involved SSEs for KIBs, as reported in Table 3.

4. Solid-state electrolytes for calcium-ion batteries

CIBs have emerged as attractive candidates for next-generation energy storage systems. CIBs are considered as a viable alternative to LIBs technology thanks to their high gravimetric and volumetric theoretical specific capacities, that surpass those of KIBs, ZIBs, and SIBs [95–97]. Calcium is ranked the 5th abundant element in earth's crust. It is commercially available, safe, nontoxic, and cost-effective. The reduction potential of Ca is high around 2.87 V vs. standard hydrogen electrode (SHE), close to Li and lower than Mg (3.04 V and 2.37 V vs. SHE, respectively). Despite the advantages listed above, mounting an efficient CIB as revealed in Fig. 8a, is not evident [98]. The development of CIBs is hindered by the lack of suitable electrolyte. Aurbach et al. [99] have recently demonstrated the ability of calcium to reversibly deposit in the presence of liquid electrolytes. The calcium metal is incompatible with the conventional non-aqueous electrolytes reported for sodium and lithium technologies. Calcium salts commercially available are few including calcium tetrafluoroborate, calcium bis(trifluoromethanesulfonyl) imide, calcium nitrate and calcium borohydride. Calcium perchlorate presents a serious safety issue and for that reason, it cannot be employed [100].

Very few studies concerning solid states state and SPE have been reported for CIBs. The reason is that Ca^{2+} diffusion is very slow for practical applications. In 2011 and 2012, CaF_2 was investigated as a solid electrolyte for different calcium-alloys such as Ca–Mg, Ca–Bi and Ca–Sn. CaF_2 have the property to became a mixed conductor at high temperatures (T > 873 °C but was never reported for the conventional battery systems [101–103]. Metal borohydrides with the chemical formula $A_xB_nH_n$ (A: Li, Na; x = 1, 2; n = 11, 12) MB_nH_n (M: Ca, Mg; n = 11, 12) were proposed as a potential candidates for solid state batteries, and Lu et al. have conducted DFT calculations in this regard. According to their findings, metal borohydrides are not stable under electrochemical oxidation and tend to be oxidized at high temperatures. The decomposition products form a protective layer at the electrode interface offering an improved electrochemical stability. It was concluded that Metal borohydrides are potential candidates to Lithium and sodium batteries. However, for divalent ions such as Mg^{2+} and Ca^{2+}, the improvement of the diffusion constant is still needed to be improved for practical application [104].

Genier et al. [105] studied poly (ethylene glycol) diacrylate as a polymer electrolyte for calcium batteries. The poly(ethylene glycol) diacrylate was photo-crosslinked under blue light in the presence of calcium nitrate and formed a stable network. In general, increasing the salt loading led to an increase in IC (Fig. 8b_1). The TGA curves presented in Fig. 8b_2 show a similar trend. The decomposition temperature is higher than 130 °C. Wang et al. [106] have proposed a PTHF-Epoxy system as a polymer electrolyte for calcium batteries (Fig. 8c_1). The solid polymer was synthesized via the copolymerisation of PTHF with a cycloaliphatic epoxy loaded with calcium nitrate as Ca^{2+} source. The properties of the GPE are strongly dependent on the salt loading. They figured out that a loading of 1.9:1 allows the highest IC in the temperature range 30–110 °C. Later, they confirmed by Raman spectroscopy that the extra solvated Ca^{2+} is the reason behind the good conductivity. In addition to that, the gel polymer was stable in a wide temperature range (Fig. 8c_2).

Martinez-Cisneros et al. [107], in 2020, have investigated three calcium salts hosted in poly(oxyethylene) as a solvent-free polymer electrolytes for calcium batteries. It has been found that introducing the salts increases the temperature of the weight loss by 100 °C. Koettgen et al. [108] studied the ability of $CaB_{12}H_{12}$ of being a solid electrolyte for calcium batteries via ab initio calculations (Fig. 8d). This group reported that doping the Ca with Al, Bi or rare-earth elements creates calcium vacancies and thus, enhancing diffusion kinetics. They emphasized that, the core repulsion of Ca^{2+} with the host's electron density is the main responsible factor for the migration barrier.

The studies reported in the literature concern only the physical and chemical properties of solid or polymer electrolyte. Nevertheless, no concrete application in the battery system is reported yet. The calcium technology is still at the infancy state. Still the appropriate liquid electrolyte in terms of safety and efficiency is not reported yet. The calcium oxide passivation layer that is usually formed on the calcium anode is highly stable and present a serious concern. In addition, the calcium ions are sluggish which makes the diffusion process more complicated. More attention should be directed toward electrolytes for calcium batteries, either liquid or solid and polymer-based electrolyte.

5. Solid-state electrolytes for magnesium-ion batteries

MIBs have shown interesting advantages as a potential divalent substitute to LIBs [109–111]. However, one of the greatest challenges to overcame to advance R&D of magnesium ion technology is the development of compatible, stable and ion-conductive electrolytes [112]. Magnesium salts such as $MgClO_4$ dissolved in conventional carbonate-based solvents react with magnesium metal to create a tick and insulating passivation film on the electrode surface, and thereby inhibits magnesium diffusion and deposition leading to a severe capacity fade [113–116]. This phenomenon was also observed to increase if the electrolyte is contaminated by even few ppm of water [117]. Consequently, novel electrolytes have gained huge attention to develop Magnesium batteries. Among them, electrolytes based on Grignard

Table 3
Summary of physical, chemical, and electrochemical parameters of SSEs for KIBs.

Electrolyte	Composition	Synthesis Method	Conductivity (S cm ^{1})	Flexibility (F: Flexible |NF: Non-flexible)	E_a (kJ mol ^{1})	Positive electrode	Negative electrode	Cell configuration	Voltage range (V)	Average voltage (V)	Initial CE @ Current density (A/g) or rate	Cycling stability [Capacity (mAh/g) @ Cycle number @ Current density (A/g) or rate]	Rate capability [Capacity (mAh/g) @ Current density (A/g) or rate]	Ref.
Inorganic	$K_3Sb_4O_{10}(BO_3)$	Solid state reaction in air at 950 °C for 48 h	1.5×10^{4} at 400 °C	NF	31.35									[90]
Organic	polypyrrole@wiper cloth	Oxidative polymerization	3.7×10^{2} at RT	F		$KFe_2(CN)_6$, xH_2O	$KFe_2(CN)_6$, xH_2O	3E (Ref: saturated calomel electrode (SCE))	0–1.2	0.6		44 @ 200 @ 0.5	28 @ 2	[91]
Inorganic	K_2Fe4O_7	Hydrothermal reaction	5×10^{2} at RT	NF	7.70	$KFe_2(CN)_6$, xH_2O	$KFe_2(CN)_6$, xH_2O	2E (Coin cell)	0–3			55 @ 50 @ 10C	53 @ 30C	[89]
Hybrid	Poly (ethylene oxide)-bis (flourosulfonyl) imide (PEO-KFSI SPE)	Dry hot-pressing approach	2.7×10^{4} at 60 °C	F		Ni_3S_2@Ni	Potassium metal	2E (Coin cell)	0.01–3 at 55 °C		97% @ 0.025	312 @ 100 @ 0.025		[87]
Inorganic	K_2CdO_2		2.2×10^{5} at RT	NF	40.52	Potassium metal	Potassium metal	2E (High-temperature Swagelok cell)						[92]
Inorganic	$K_{2.9}Ba_{0.05}OI$	Solid state reactions	3.5×10^{3} at 270 °C	NF	34.73	Potassium metal	Potassium metal	2E (Coin cell)						[93]
Hybrid	The Poly (propylene carbonate) (PPC)–KFSI with cellulose nonwoven backbone SPE (PPCB-SPE)	Solution-casting method	1.36×10^{5} at 20 °C	F		3,4,9,10- perylene-tetracarboxylicacid-dianhydride (PTCDA)	Potassium metal	2E (Coin cell)	1.5–3.5	2.3		104 @40 @ 0.010	79 @ 0.1	[86]
Hybrid (Quasi-solid)	Perfluorinated sulfonic acid membrane (PFSA-K) impregnated with KPF6	Solution blade coating method followed by drying	9.36×10^{5} at 25 °C	F		PTCDA	graphite	2E	1.5–3.5	2.4	97.5 @ 0.1	84 @ 200 @ 0.1 (15 °C)	90.9 @ 0.8	[83]
Inorganic	KSi_2P_3	Solid state reaction under inert conditions	5×10^{2} at RT	NF	19.3	Ruthenium (as ion-blocking electrode)	Ruthenium (as ion-blocking electrode)	2E (RHD INSTRUMENTS Microcell HC)						[94]

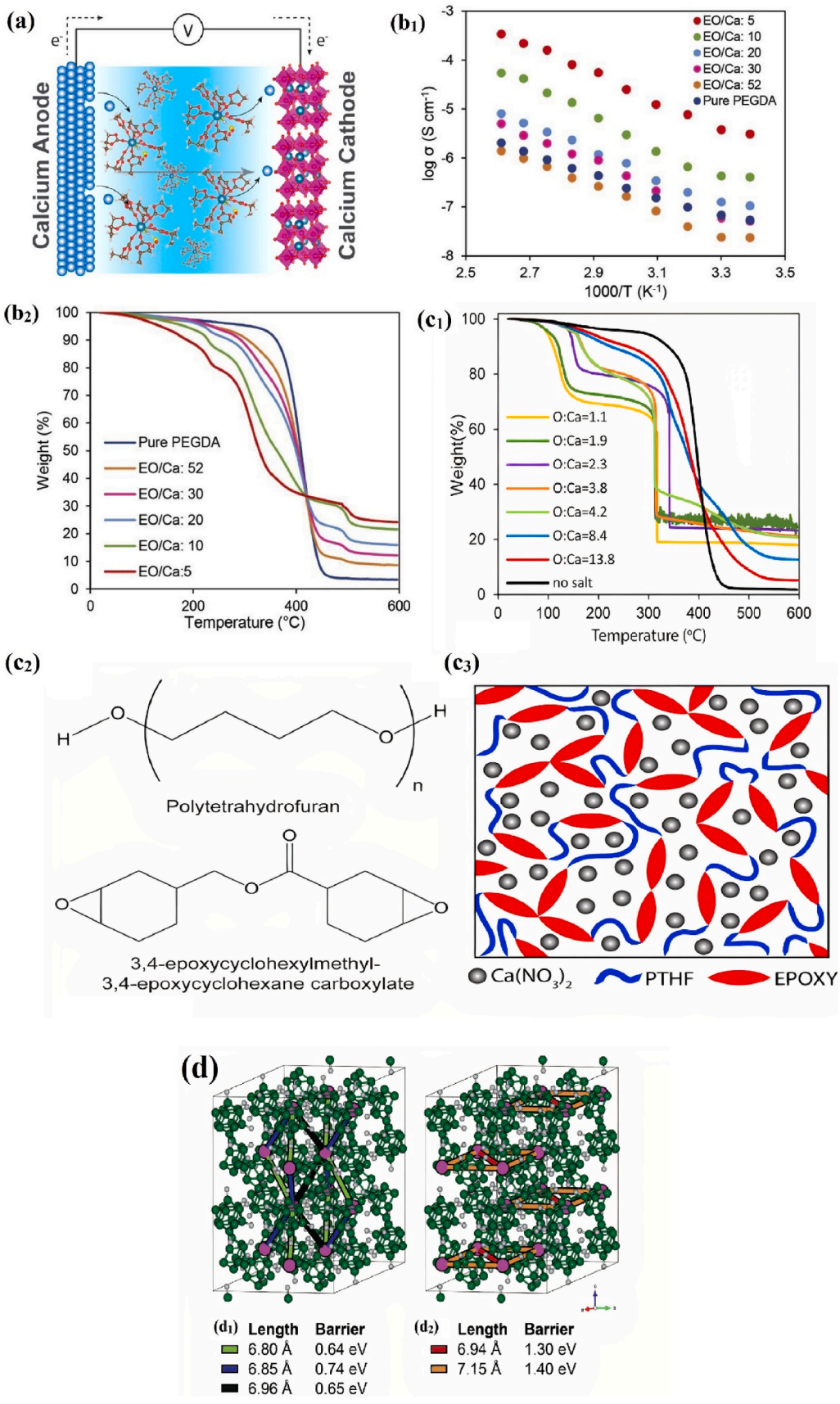

Fig. 8. (a) Schematic illustration of a CIB cell [98] (Copyright 2021, ASC). **(b_1)** Ion conductivity of PEGDA-Ca crosslinked networks in Arrhenius plots over a range of salt loadings, **(b_2)** TGA plots of pure PEGDA crosslinked networks and salt-loaded samples with different EO/Ca ratios [105] (Copyright 2019, Elsevier). **(c_1)** Precursors for PTHF−Epoxy Cross-Linked Networks, **(c_2)** Schematic of the Cross- Linked Structure, **(c_3)** TGA curves of a pure PTHF−Epoxy sample and salt-loaded SPEs [106] (Copyright 2019, ASC). **(d)** $CaB_{12}H_{12}$ structure and possible migration paths, **(d_1)** Paths between layers, **(d_2)** paths within the layers [108] (Copyright 2020, RSC).

compounds dissolved in aprotic solvents [118], ionic-liquid electrolytes [119,120] and SSE [121–123] are the most studied.

SSEs are regarded as a stable alternative. However, the relatively poor conductivity at RT remains a critical issue to fix as magnesium ions are tightly bonded within their crystallographic lattice sites, especially at low temperature. In this part, we will present an overview of various SSEs that enable Mg ions conduction, classified into three groups: ceramics, polymers, and composite. Then, the discussion and comparison of their characteristics, in terms of IC, transport number, electrochemical and thermal stability if available as well as their mechanical strengths, will be presented.

5.1. Ceramics

The first investigation of magnesium ion conducting in the system Mg-Zr-PO (MZP) dates to 1987, when Ikida et al. studied various compositions of Mg:Zr:PO_4 synthesized using conventional solid-state method and showed that $MgZr_4(PO_4)_6$ which crystalizes in NASICON-type crystal structure with rhombohedral symmetry has the best IC among all. Its conductivity was determined to be 2.9×10^{-5} at 400 °C and 6.1×10^{-3} S cm^{-1} at 800 °C. The authors used Tubandt's method along with electron probe micro analysis to approve that the charge carriers in this material are magnesium ions [124]. The $MgZr_4(PO_4)_6$ crystal structure was later deeply investigated by Kazakos-Kijowski and co-authors [125]. The material was synthesized using sol-gel method and calcined at lower temperature compared to solid-state method. The XRD results revealed that $MgZr_4(PO_4)_6$ crystalizes in the monoclinic system (alike β-Fe_2SO_4) rather than in the rhombohedral system. A comparison between the IC in both NASICON-type and β-iron sulfate-type $MgZr_4(PO_4)_6$ compounds using first-principles molecular dynamics (FPMD) has been reported recently by Kanamura and co-authors [126]. The time-averaged mean square displacement (MSD) showed that in both structures, only magnesium ions diffuse in the lattice (the structures are represented in Fig. 9 a_1). However, the FPDM calculations revealed that NASICON type has a superior IC than that of β-iron sulfate-structure as a result of the reduced magnesium migration energy in the former compared to the latter (Fig. 9 a_2). Despite that, the conductivity of $MgZr_4(PO_4)_6$ is still low for practical application. Therefore, In 2000 Imanaka et al. reported some new modifications on $MgZr_4(PO_4)_6$ in order to improve its IC by forming a microscopic dispersion of $ZrO(PO_4)_2$ in the mother compound $Mg_{1.4}Zr_4P_6O_{24.4}$ and thereby, the IC increased to reach 6.92×10^{-3} S cm^{-1} at 800 °C owing to the enhancement of the relative density compared to the mother phase $MgZr_4(PO_4)_6$ [127]. Or by substituting the tetravalent Zr^{4+} ions for pentavalent Nb^{5+} in $MgZr_4(PO_4)_6$ to obtain $Mg_{0.7}(Zr_{0.85}Nb_{0.15})_4(PO_4)_6$ which results in statistical distribution of the mobile Mg^{2+} ions in the three occupying sites, a considerable enhancement of Mg^{2+} ion conductivity [128,129] is noticed. Nevertheless, the E_a of magnesium ions migration becomes high which reduces the IC at lower temperature. Therefore, Tamura et al., tried to synthesize NASICON type structure of magnesium ion conductor in order to reduce the E_a. However, all the attempts were unsuccessful, and they ended up getting β-Fe_2SO_4-type solids. Although, they were able to develop a three-dimensional well-ordered NASICON-type magnesium cations conductor by substituting Hf^{4+} with Mg^{2+} in $HfNb(PO_4)_3$ [130], The resulting IC was 20 times higher (2.1×10^{-6} S cm^{-1}) to the previously reported $Mg_{0.7}(Zr_{0.85}Nb_{0.15})_4(PO_4)_6$ (1.1×10^{-7} S cm^{-1}) at relatively low temperatures around 300 °C. The authors believe that this improvement is owing to the reduced E_a for magnesium migration in $(Mg_{0.1}Hf_{0.9})_{4/3.8}Nb(PO_4)_3$ which has an ordered structure compared to the conventional β-Fe_2SO_4 structure. Based on this, the substitution of Zr and P atoms in the mother phase $Mg_{0.5}Zr_2(PO_4)_3$ by other elements has become another way to enhance the magnesium ions conduction in this compound. Several dopants have been reported such as Si [131], Nb [132], Ce [133], Sn [134] or double substitution [135] like implementing Zn^{2+} and Al^{3+}. The XRD pattern revealed that the complete substitution of Zr by Si results in $Mg_{0.5}Si_2(PO_4)_3$ with a monoclinic structure. $Mg_{0.5}Si_2(PO_4)_3$ sintered at 800 °C showed a higher conductivity at ambient temperature in comparison to $Mg_{0.5}Zr_2(PO_4)_3$ (1.06×10^{-6} S cm^{-1} vs. 5×10^{-13} S cm^{-1}) as depicted in Fig. 1 b_1. This enhancement is ascribed to the decrease of the lattice parameters resulting from the substitution of Zr (0.72 Å) with Si (0.41 Å) which provided an appropriate tunnel size for the migration of magnesium ions. Moreover, the linear sweep voltammetry was used to study the stability of this compound as an electrolyte. The voltammogram showed (Fig. 9 b_2) that $Mg_{0.5}Si_2(PO_4)_3$ is stable up to 3.2 V which is beyond the stability window required for an electrolyte in magnesium ion batteries. However, the cell assembly details are not reported in this study [131]. The IC at RT has further improved by double complete substitution of Zr with smaller Al and Zn to form the composition $Mg_{1.05}Zn_{0.4}Al_{0.3}Zr_{1.3}(PO_4)_3$ with a better IC at RT [131].

Different metal hybrids were also studied as a SSE candidate for MIBs, as they are strong reductive agents presenting a high stability against the electrochemical reduction of the negative electrode [136,137]. In 2012, Matsuo and co-workers reported first-principles molecular dynamics (FPMD) simulations on possible magnesium conduction in the phase of Mg $(BH_4)_2$. They showed that magnesium is situated in small tetrahedral cage made by four $[BH_4]^-$ with strong coulombic interactions which limited the magnesium ions migration. Therefore, the authors suggested that by doping some of $[BH_4]^-$ by larger $[AlH_4]^-$ could improve the ionic conduction (Fig. 9c) [138]. Higashi et al. proved the ionic bonds of Mg (BH_4) (NH_2) (structure illustrated in Fig. 9 d_1) with a gap energy of about 4.9 eV through DFT calculation. The higher ionic conduction of 1×10^{-6} S cm^{-1} at 150 °C of Mg(BH_4) (NH_2) compared to $Mg(BH_4)_2$ is attributed to the small distance between nearest neighbouring magnesium atoms about 3.59 Å. The thermal evolution of the IC of $Mg(BH_4)_2$, Mg(BH_4) (NH_2), $MgZr_4(PO_4)_6$ and $Mg_{1.4}Zr_4P_6O_{24.4}$+$0.4Zr_2O(PO_4)_2$ is illustrated in Fig. 9 d_2 [139]. The IC was observed to increase by adding a neutral bidentate ethylenediamine ligand $(NH_2CH_2CH_2NH_2)$ in magnesium borohydride via mechanochemical reaction which has an IC of 5×10^{-8} S cm^{-1} at 30 °C and 6×10^{-5} S cm^{-1} at 70 °C. The authors proved the stripping/deposition of magnesium ions at 60 °C in Pt/Mg(en)$_1$$(BH_4)_2$/Mg cell using cyclic voltammetry [140]. ICs of 10^{-5} S cm^{-1} and 10^{-3} S cm^{-1} at RT and at moderate temperature (ca. 70 °C),respectively were achieved by the realization of composite of two crystalline compounds to get Mg $(BH_4)_2$·$1.6NH_3$ [141].

The first discovery of trinary spinel chalcogenides with high magnesium mobility was reported in 2017 by Canepa and co-authors [142]. The authors proposed that residing magnesium in its unfavorable site different (i.e., tetrahedral site) than in octahedral site along with expanded volume per anion $O^{2-} > S^{2-} > Se^{2-} > Te^{2-}$ contribute to a lower migration barrier leading to a fast motion of magnesium ions. These finding leads the authors to investigate chalcogenide-based spinel compounds with stoichiometry MgX_2Z_4 (where Z = S and Se and X = In, Y and Sc). DFT-based nudged elastic band (NEB) calculations showed that MgY_2Se_4 and $MgSc_2Se_4$ have the lowest migration barrier (~361 meV for MgY_2Se_4 and ~375 meV for $MgSc_2Se_4$), as illustrated in Fig. 9 e_1. The high magnesium conduction in $MgSc_2Se_4$ was confirmed by Mg single sharp NMR relaxometry along with electrochemical impedance spectroscopy which equals to 0.1 mS cm^{-1} at RT. However, the impedance spectroscopy (Fig. 9 e_2) showed also an appreciable electronic conductivity about 4×10^{-8} S/cm which is larger in comparison to other SSE for LIBs [143]. Therefore, in order to obtain a practical solid-state magnesium electrolyte, approaches to suppress the high electronic conductivity in $MgSc_2Se_4$ are needed. Later on, the same group explored the defects structure of $MgSc_2Se_4$ using first-principles calculations in order to pinpoint the reason behind this relatively high electronic conductivity [144]. The authors revealed that the samples synthesized under anion excess and slow cooling are expected to have the lowest electronic conductivity. Based on this, Fichtner and co-workers in 2019 reported two different attempts to overcome the

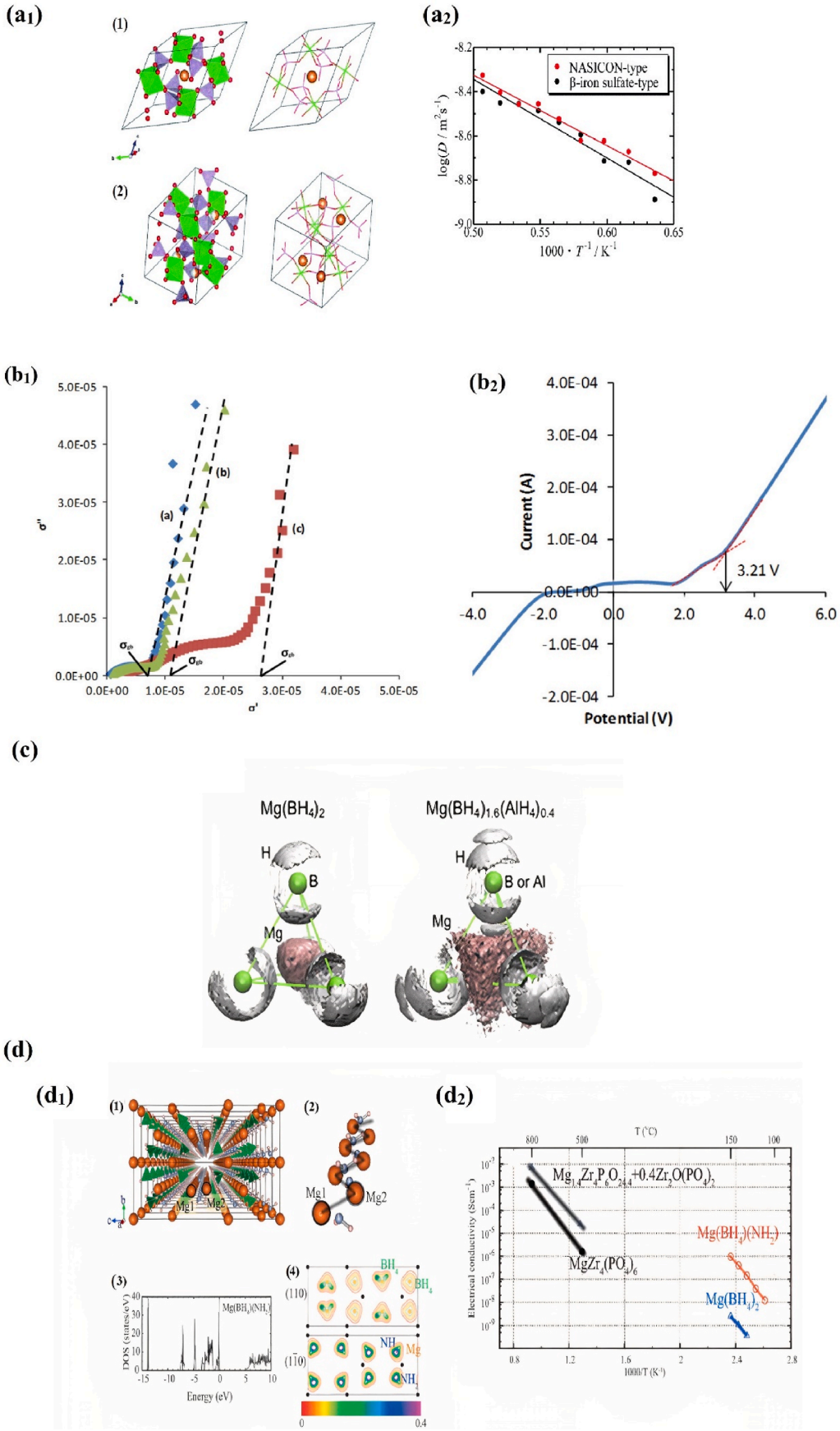

Fig. 9. (a_1) 1) MZP with a NASICON-type structure 2) MZP with β-iron sulfat, **(a_2)** Arrhenius plots of Mg-ion diffusion coefficients [126] (Copyright 2019, RSC). **(b_1)** Conductivity spectra plot of $Mg_{0.5}Si_2(PO_4)_3$ at (a) 700 °C (b) 800 °C and (c) 900 °C, **(b_2)** Linear sweep voltammogram of the $Mg_{0.5}Si_2(PO_4)_3$ [131] (Copyright 2016,

Elsevier). **(c)** Iso-chemical potential (0.18 eV) surface of Mg and H atoms calculated by FPMD at 500 K for the high temperature phase of (left) $Mg(BH_4)_2$ and (right) $Mg(BH_4)_{1.6}(AlH_4)_{0.4}$ [138] (Copyright 2016, Elsevier). **(d_1) 1)** Structure of $Mg(BH_4)(NH_2)$. **2)** Mg zigzag structure from **1)**. **3)** Electronic density states of $Mg(BH_4)(NH_2)$. **4)** Valence charge contour plots. **(d_2)** Thermal evolution of IC of $Mg(BH_4)_2$ and $Mg(BH_4)(NH_2)$ [139] (Copyright 2014, RSC). **(e_1)** First-principles calculations in sulfides, selenides, and tellurides AX_2Z_4 spinels. **1)** migration path in the AX_2Z_4 framework. **2)** Effect of the anion size on the shared (triangular) face. **3)** and **4)** computed Mg and Zn migration barriers in AX_2Z_4 spinel. **5)** Mg probability density in $MgSc_2Se_4$ at 900 K. **6)** Mg diffusivities in $MgSc_2Se_4$ and MgY_2Se_4. **(e_2)** Impedance spectrum of the Ta/$MgSc_2Se_4$/Ta cell [142] (Copyright 2017, Nature). **(f)** SEM image of the ball-milled mixture and elements distribution [145] (Copyright 2021, Elsevier).

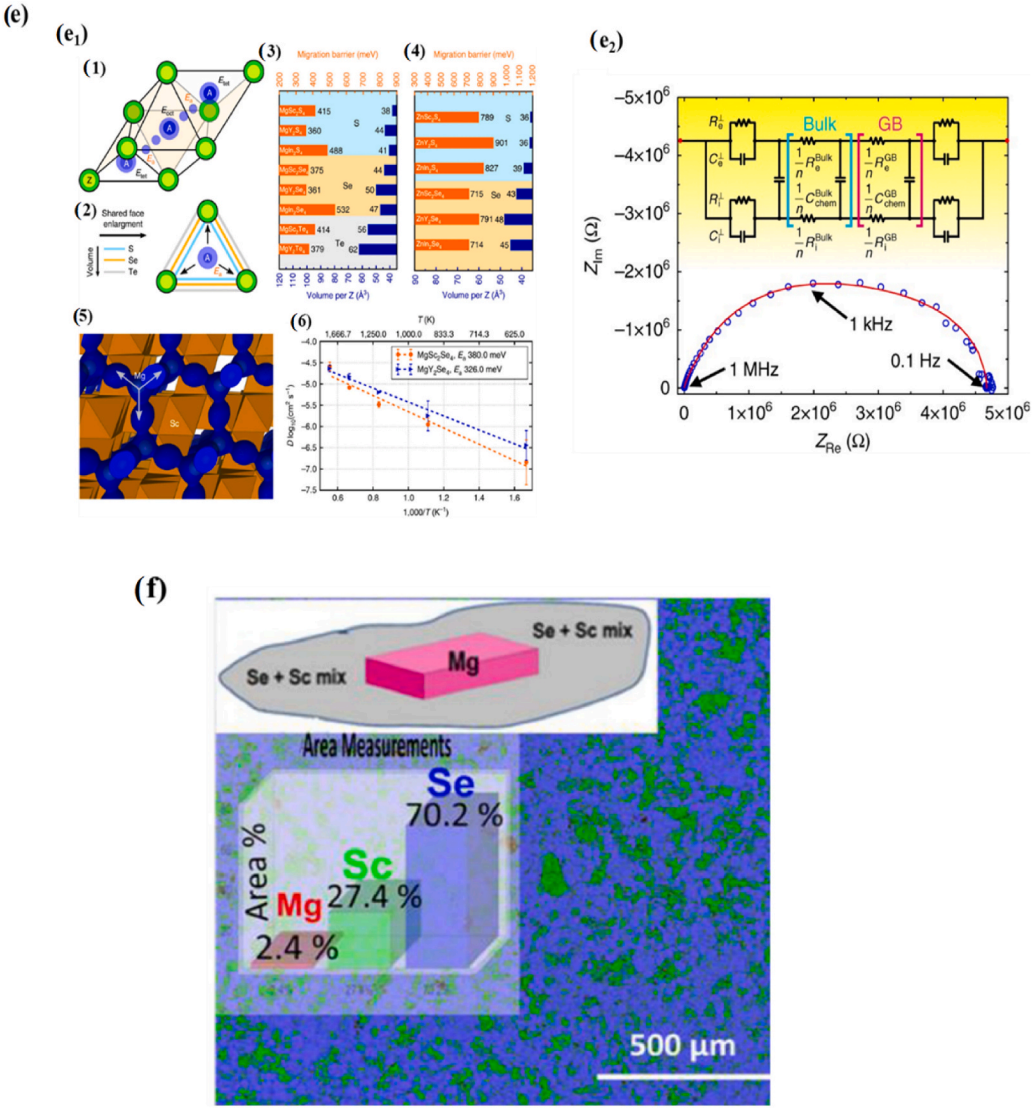

Fig. 9. (*continued*).

high electronic conductivity of $MgSc_2Se_4$, where they described the synthesis of Se-enriched $MgSc_2Se_4$ and doping of Sc^{3+} by Ti^{4+} and Ce^{4+} compounds using a solid-state reaction. However, they revealed that excess of 5% of selenium could just slightly lower the EC and maintains the same IC of the pure materials while increasing the selenium excess up to 10% leads to an increase of the electronic conductivity meaning that the anion excess cannot suppress the electronic conductivity in $MgSc_2Se_4$. Moreover, they claimed that even the substitution of Sc^{3+} by Ti^{4+} and Ce^{4+} did not show any improvement suggesting that other strategies are highly required for further enhancement, instead the authors proposed the use of this type of materials as electrodes for MIBs owing to their high IC and EC. Two years later, Kundu et al., presented an efficient understanding of the electronic conduction mechanism in $MgSc_2Se_4$ spinel and its correlation with the morphology of the material [145]. The authors showed that the electronic conductivity in Mg-Sc-Se ceramic follow the Berthelot-type conductivity model which suggests that the formation of nano-sized Sc/ScSe conducting compounds around the particles (See Fig. 9f) during the ball milling process helps the electrons tunnelling and therefore originates high electronic conductivity. In addition, the authors proved that avoiding ball milling of the precursors mix serves to decrease the electronic conductivity at RT [145].

5.2. *Polymers-based electrolytes*

Polymer-based SSEs are examined as potential candidate for SSE owing to their high safety, high mechanical and shape flexibility, non-volatility as well as high thermal stability. Polymer-based electrolytes are classified into two groups SPEs and GPEs. SPE consist of dispersing a salt into a polymeric matrix. Like liquid electrolytes, the alkali metal ions transport is only possible when the salt is dissociated which is highly depends on the salt to polymer concentrations ratio. However,

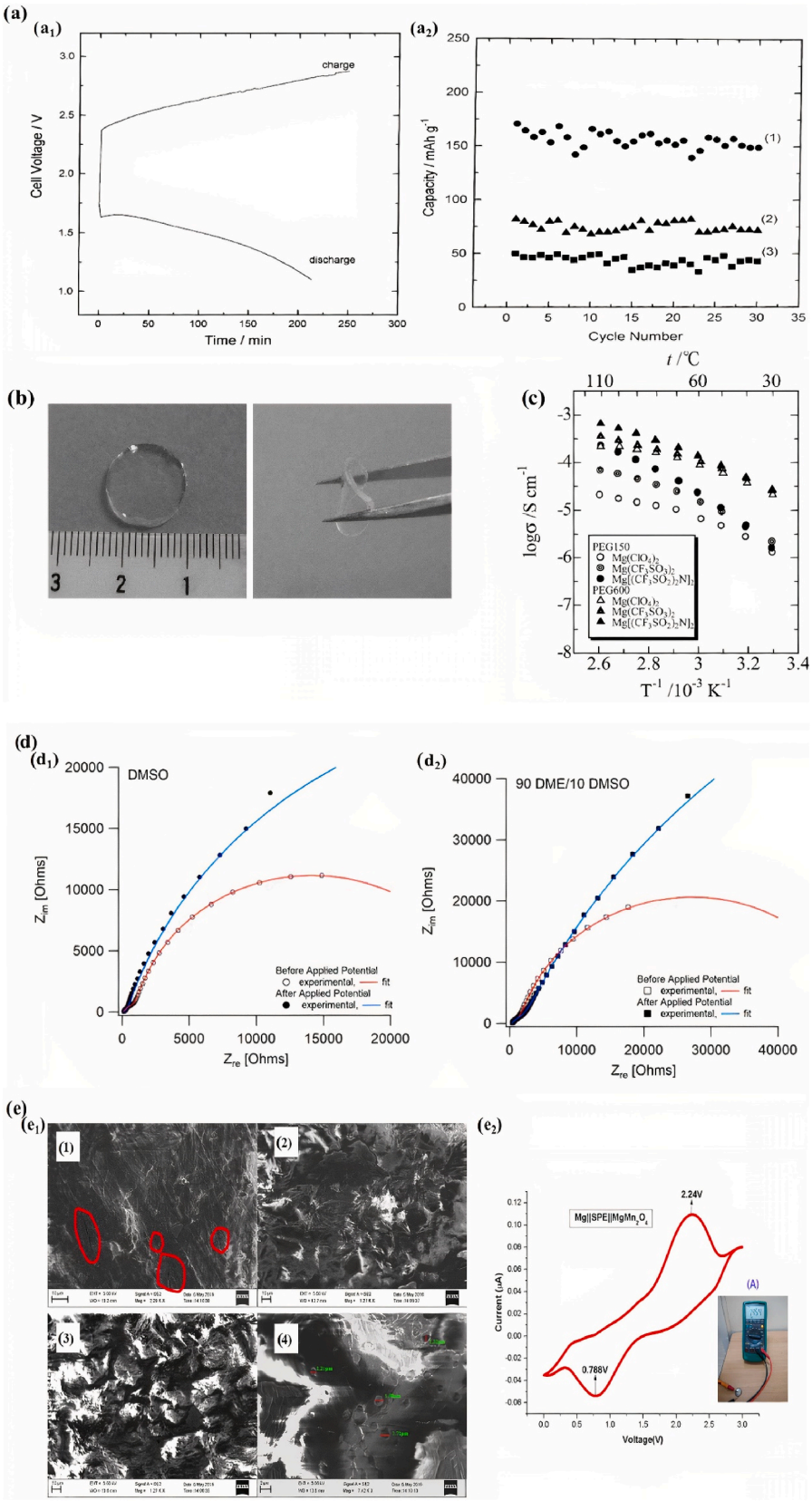

Fig. 10. **(a_1)** Voltage vs. time of Mg/GPE/MnO_2 cell. **(a_2)** Capacity vs. cycke number of Mg/GPE/MnO_2 at different C-rates [163] (Copyright 2001, Elsevier). **(b)** Pictures of polymeric gel film: (PEO–PMA)–(EC + DMC)/Mg[$(CF_3SO_2)_2N]_2$ [152] (Copyright 2001, Elsevier). **c)** Arrhenius plots for IC of PEGx-B_2O_3 +MgX_2 [154] (Copyright 2003, ACS). **(d_1)** EIS spectra of Mg/Mg cells with DMSO. **(d_2)** EIS spectra of Mg/Mg cells with 90 DME/10 DMSO swelled polymer film [156] (Copyright 2019, ACS). **(e_1)** FE-SEM images of **1)** PEO **2)** PEO-PVP **3)** and **4)** SPE-Mg30, **(e_2)** CV curve of the assembled Mg ion cell [159] (Copyright 2017, Elsevier). **(f_1)** The preparation process of the PPE. **(f_2) 1)** Rate capabilities of MoS_2/C//PPE//Mg at various current densities. **2)** Cycling performances of MoS_2/C//Mg batteries with different electrolytes. **3)** Long-cycling stability of MoS_2/C//PPE//Mg [162] (Copyright 2021, Elsevier).

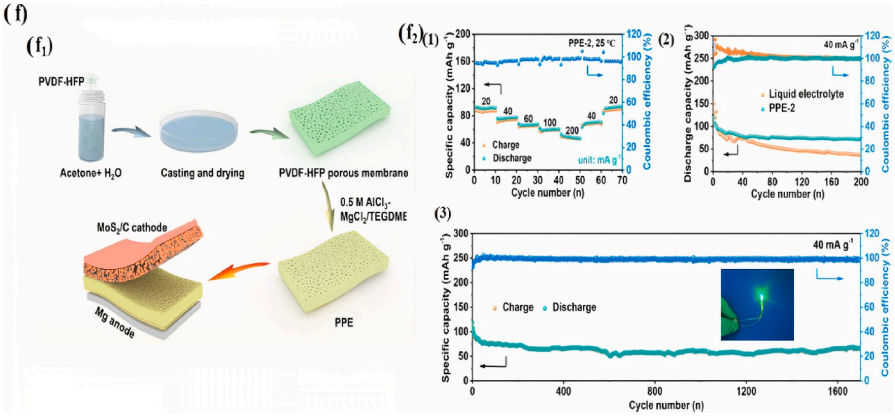

Fig. 10. (*continued*).

the low ionic conduction and cationic t_{Mg}^{2+} still a huge drawback of SPE. While in GPE, an amount of salt dissolved in an organic solvent is added to the polymer matrix which results in a gel, thus facilitates the contact with the electrodes in comparison to SPE, but the mechanical flexibility is a real concern in this case [146,147].

The first synthesis and investigation of polymer electrolyte for magnesium ion batteries was performed by Acosta and Morales in 1997, when they synthesized an electrolyte based on mixing polyether blends PEO, PPO and PPz with magnesium trifluoromethane sulfonate. However, the ICs of the samples were about 10^{-8} at low temperatures (50 °C) [148]. A high IC in the order of 10^{-5}-10^{-4} S cm^{-1} at 60 °C is reached by Liebenow in 1998 by dissolving different volumes of Grignard reagent ethyl magnesium bromide (EtMgBr) in PEO resulting in a gel like compositions [149]. Girish Kumar and co-author synthesized a GPE for MIBs by mixing magnesium trifluoromethane sulfonate, propylene carbonate and ethylene carbonates with two different polymers PAN and PVDF showing a superior IC alike liquid electrolytes, the impedance results revealed an IC of 1.8×10^{-3} S cm^{-1} and 2.67×10^{-3} S cm^{-1} at 20 °C for PAN [150] and PVDF [151], respectively,. Nevertheless, the mechanical performances are poor compared to SPE due to the existence of PC and EC solvents. Mg//MnO_2 cell using PVDF-based gel electrolyte shows a capacity of about 160 mAh/g at C/8 which remains constant during 30 cycles and then starts to decrease due to the poor efficiency of magnesium insertion into MnO_2 cathode as presented in Fig. 10 a [151]. Yoshimoto et al. presented a self-standing gel polymer based on dissolving ($Mg[(CF_3SO_2)_2N]_2$) in PEO-modified PMA matrix plasticized with EC and DMC (Fig. 10b). The polymer has an IC in the range of 10^{-3} at RT, which increases with increasing the amount of plasticizer used [152]. An IC equals to 4.8×10^{-3} S cm^{-1} at 20 °C was achieved for a gel polymer of 1-ethyl-3-methylimidazolium trifluoro-methane sulfonate ionic liquid and magnesium salt solution in PVdF-HFP. The GPE has a high mechanical strength, flexibility and good thermal and electrochemical stability. However, the transport number of magnesium is relatively low about 0.26 which limited its practical use [153]. In an early study and in order to enhance the t_{Mg}^{2+}, Saito and co-authors clarified the impact of Lewis acid and the anion species of the salt in the cationic transport number, they reported the synthesis of a novel solid polymer electrolyte consisting of incorporating three different salts Mg$(ClO_4)_2$, Mg$(CF_3SO_3)_2$, and Mg$[(CF_3SO_2)_2N]_2$ into a PEG polymer using a borate ester (Lewis acid) as a cross-linker agent. They revealed that the conductivity has been improved as illustrated in Fig. 10 c. Moreover, the t_{Mg}^{2+} was high as 0.51 for Mg$(ClO_4)_2$ compared to the other salts which is ascribed to the strong interaction between borate ester and ClO_4 anions boosting the degree of dissociation of magnesium salt (weak coulombic interactions between Mg^{2+} and ClO_4) leading to a high t_{Mg}^{2+} [154]. Recently, single ion conducting polymer electrolytes have gained an interest in solid-state batteries due to its ability in binding covalently the salt's anions to polymer backbone and thus increasing the cationic t_{Mg}^{2+}. Balsara's group reported a single-ion conducting block copolymer produced from the polymerization of PEO P(STFSI) and then dialysis process with magnesium chloride ($MgCl_2$) to form PEO P[(STFSI)$_2$Mg]. Vogel Tamman Fulcher (VTF) relation proved that magnesiated polymer has a lower ion dissociation compared to its lithium analogues. Moreover, the ionic conduction was very low [155]. Three years later, Laura and co-authors used co-polymerization of PEO dimethacrylate (PEGDMA) with potassium 4- styrene sulfonyl (trifluoromethyl sulfonyl) imide (KSTFSI) monomer in dimethyl sulfoxide (DMSO) solvent to produce a single-ion conducting magnesium GPE. The latter has an IC approaching 10^{-4} S cm^{-1} at 25 °C. However, the impedance shows a high charge transfer resistance corresponding to desolvation of magnesium ions preventing the reversible deposition of magnesium metal (Fig. 10d) [156].

Several SPEs have been studied as SSEs for MIBs, where their relative IC is in the range of 10^{-5} - 10^{-4} at RT [157–160]. In 2017, Anilkumar and co-workers investigated the suitability of blend polymer based on solvating PEO and PVP with several concentration of Mg$(NO_3)_2$ salt in solid-state MIBs. The SEM images revealed the smooth particle surface of the SPE membrane compared to pure PEO besides the formation of micro pores which is a useful in thing a separator membrane (Fig. 10 e_1). The self-standing SSE has the highest IC among all reported SPEs which is around 5.8×10^{-4} S cm^{-1} at RT with t_{Mg}^{2+} of 0.33. Furthermore, it was proven that it is electrochemically stable from 0 to 4 V. The cyclic voltammetry of Mg//SPE membrane//$MgMn_2O_4$ cell, shown in Fig. 10 e_2, exhibits two distinct peaks indicating the electrochemical activity of the SPE membrane [159]. Ponraj and co-authors studied the impact of adding a plasticizer on the conductivity of SPE composed of copolymer poly(vinylidene chloride-co-acrylonitrile-co-methyl methacrylate) and $MgCl_2$. The IC of 70 wt% poly (VdCl-co-AN-co-MMA):30 wt% $MgCl_2$ was in the range of 10^{-5} S cm^{-1}. Although, after adding different concentrations of succinonitrile plasticizer, the IC increased to be in the range of 10^{-3} S cm^{-1} at RT [161]. Li-Zhen Fan et al. demonstrated the reversible magnesium ions plating/stripping at 0.13 V in Mg//MoS_2/C using a porous polymer electrolyte prepared by immersing porous PVDF-HFP membranes in $MgCl_2$–$AlCl_3$/TEGDME (Tetra ethylene glycol dimethyl ether) electrolytes (Fig. 10 f_1). The latter has an IC of 4.72×10^{-4} S cm^{-1} at RT with a good electrochemical stability. The cell preserves a capacity of 66 mAh g^{-1} after 1700 cycles at 40 mA g^{-1} which relatively high compared to the properties of the cell when a liquid electrolyte is used (47 mAh g^{-1} after 200 cycles) as depicted in Fig. 10 f_2, resulting from the uniform plating/stripping of Mg^{2+} and reduced side reactions [162].

5.3. Composite electrolytes

As shown throughout this part, huge attention is given to develop SSEs for magnesium ion batteries either based on inorganic materials

(ceramics) or organic ones (polymers). However, finding the suitable solid electrolyte for practical use that satisfy all the requirements is a grand scientific challenge. Therefore, composite electrolytes approach has become a new road to produce a solid electrolyte that combines the advantages of both polymers and ceramics while enables achieving a high IC, elevated cationic t_{Mg}^{2+}, low charge transfer resistance as well as high softness which enhance the electrode-electrolyte interface [164–168].

Hashmi's group studied in 2010 the impact of fumed silica dispersion on PVDF-HFP using several physical techniques. They showed that dispersing 3% of silica serves to increase the IC up to 1.1×10^{-2} S cm^{-1} at RT while having a large voltage range and high thermal stability. Moreover, when used as SSE for MIBs. The Mg-MWCNT composite//MoO_3 cell delivers a capacity of 175 mAh g^{-1} for 10 cycles (Fig. 11a). The t_{Mg}^{2+} was around 0.28 revealing that the improvement of the IC is assigned to the improvement of anions mobility [169]. The same group fabricated a nanocomposite electrolyte based on PVdF-HFP dispersed with nanosized MgO particles. The self-standing electrolyte has a conductivity of 8×10^{-3} S cm^{-1} at RT after adding 3 wt% of MgO, the t_{Mg}^{2+} seems to be improved to 0.44 after adding 10 wt% of MgO owing to the space-charge regions that facilitate the Magnesium ions mobility [170]. A nanocomposite electrolyte based on PEO, Mg $(BH_4)_2$ and MgO nanoparticles without any flammable plasticizers had been reported, the film has a smooth surface suggesting the homogeneity in the distribution of $Mg(BH_4)_2$ fillers with a thickness of 200 μm as shown in Fig. 11 b_1. The CV results indicate the reversible magnesium plating/stripping with 0.2 V as a gap between the Mg plating and Mg stripping revealing fast and reversible kinetics (Fig. 11 b_2). The authors also demonstrated that the cell configuration Mg/Mg $(BH_4)_2$–MgO–PEO/Mo_6S_8 has stable electrochemical performances over 150 cycles [171]. Using the same ceramic filler, Du et al. reported in 2019 the synthesis via in-situ crosslinking reaction of hydroxyl-terminated poly tetrahydrofuran and Mg $(BH_4)_2$ in a glass-fiber membrane in order to provide good flexibility. The synthesis procedure is illustrated in Fig. 11 c_1 where a solvated $MgCl_2$ in THF is added to the previously mentioned composition to enhance the electrochemical performances. Electrochemical impedance spectra showed that composite electrolyte has an IC of 4.76×10^{-4} S cm^{-1} at RT which is not quite high compared to some other solid electrolyte discussed above. However, it has the highest t_{Mg}^{2+} of 0.73 at RT (Fig. 11 c_2). Moreover, it has the widest operating temperature range (20–60 °C). Mo_6S_8//PTB@GF-GPE//Mg cell demonstrated an excellent electrochemical performances which a capacity retention of 97.7% over 250 cycles at 0.5C [172]. Recently, Sun and co-workers investigated PVdF-HFP- 4 wt % nanosized SiO_2–Mg-$(TFSI)_2$ as a composite electrolyte for MIBs. The electrolyte has an ionic conduction of 0.83×10^{-3} S cm^{-1} and a great compatibility with magnesium metal and $H_{0.68}Ti_{1.83}O_4{\cdot}xH_2O$ cathode [173].

6. Solid-state electrolytes for zinc-ion batteries

Large interest was dedicated lately to multivalent-ion batteries due to their advantageous cost and possible application in stationary energy storage systems, whose development is crucial for renewable energy technologies. The di- and tri-valent metal anodes (Ca, Mg, Al, Zn, etc …) in such batteries show low specific gravimetric capacities, higher reduction potential compared to lithium vs. SHE, but higher volumetric capacities, as mentioned in Fig. 1, and low cost which makes them particularly attractive. ZIBs are recognized as alternative options for the Next-generation batteries. They demonstrate high theoretical capacity of 820 mAh g^{-1}, proper working voltage around 0.76 V vs. SHE, abundant reserves and most importantly safe. However, this technology is still facing big challenges such as serious dendrite growth and consecutive side reactions which obstruct its practical application [174–176]. Furthermore, the metallic Zn anode exhibits different advantages and drawbacks depending on the ways from which Zn is stripped and/or plated. Aqueous batteries are economically more sustainable because the electrolytes are generally inexpensive, safe, ecologically friendly, and should make available RT battery assembly. However, organic electrolytes may offer better oxidative (anodic) stability compared to their aqueous counterparts, promoting high operating voltage (2–3 V) and high energy density [177]. Currently, one major factor that differentiates these systems is their kinetics, which should strongly influence the electrochemical performance that is already controlled by slow-moving solid-state diffusion of divalent Zinc [178]. To solve the aforementioned limitations, solid or QSSEs were proposed as they can successfully control the interfacial ionic transfer and the Zn platting/striping processes [179]. Using SSEs for LIBs have demonstrated that this type of electrolyte maintains a mechanical barrier which effectively limits Li dendrite growth [84,180]. For this reason, SSEs are suitable to promote the use of metallic Zn as anodes and enhance their electrochemical properties. In comparison, there are few publications on SSEs for ZIBs due to the robust electrostatic character between Zn^{2+} ions and as consequence, resulting in slow diffusion kinetics [181].

SPEs are prepared by the complexation of a chosen zinc salt in a polymeric matrix. Wang et al. [181] developed a nCPE composed of aramid nanofibers (BANFs), PEO, and $Zn(CF_3SO_3)_2$. The good mechanical properties of the BANF network effectively inhibit dendrite growth. Moreover, this combination has significantly improved the IC to 2.5×10^{-2} mS cm^{-1}. Other formulations were reported such as, PVDF/PEO-$Zn(CF_3SO_3)_2$ [182] and PEO/$Zn(CF_3SO_3)_2$ + xZnO [183]. Nevertheless, they show low ICs in the range of 10^{-2} mS cm^{-1}. Wang et al. [184] reported a synthetic modified metal organic framework water@ZnMOF-808 for ZIBs. MOF are porous materials, cationic Zn $(H_2O)_6^{2+}$ are formed after filling the pores with H_2O molecules. This electrolyte shows a high IC of 2.1×10^{-1} mS cm^{-1}, due to the highly concentrated $Zn(H_2O)_6^{2+}$ ions. A lower E_a of 0.12 eV, and high t_{Zn}^{2+} of 0.93, as well as good mechanical and electrochemical properties were obtained. Additionally, due to the huge number of solid microporous structure involving good interface properties between the zinc metal and the SSE. It is highly compatible with zinc metal anode where a soft zinc deposition layer without the formation of Zn dendrites. Excellent properties of the studied SSE were confirmed in a VS_2/Zn cell configuration exhibiting good capacities of 125 mAh g^{-1} after 250 cycles and 50 mAh g^{-1} at 0.2 A g^{-1} and 2 A g^{-1}, respectively (Fig. 12 a_1–a_3). SPE composed of PVDF-HFP/PEO matrix and zinc tetrafluoroborate Zn $(BF_4)_2$ salt was studied. $Zn(BF_4)_2$ is highly soluble in [EMIM]BF_4 ionic liquid [185]. High concentration of Zn^{2+} ions is expected inducing high IC of around 16.9 mS cm^{-1} at RT. Furthermore, the [EMIM]BF_4 ionic liquid ensures good protection of the Zn metal as revealed by dendrite-free Zn stripping/plating after 3000 cycles at 2×10^{-3} A cm^{-2} with a CE of 100%.

The use of SSEs for ZIBs is very restricted because of their slow diffusion kinetics of Zn^{2+} and low ionic mobilities. To solve these problems, GPE were proposed where their preparation relies on mixing zinc salt and a polymer. The water-generated side reactions (i.a. hydrogen evolution and by-products) will be avoided due to the lower content in water molecules. Consequently, the diffusion kinetics will be improved via the formation of interactions between Zn^{2+} ions and the functional groups within the gel. These interactions blocks the free migration of Zn^{2+} which causes dendrite formation [186]. Zhi's group [187] synthesized a GPE combining zwitterionic sulfobetaine and cellulose. High IC was obtained around of 24 mS cm^{-1} mainly attributed to the facile charge transfer between the charged groups and the electrolyte ions. Moreover, the ion transport in the electrolyte is eased via the zwitterionic groups on the sulfobetaine chains which induces ion migration channels for anions and cations. At 1C and 30C-rates, reversible capacities of 275 mAh g^{-1} and 74 mAh g^{-1} were delivered after 10 000 cycles. Qingxin et al. [188] reported a hydrogel electrolyte with self-healing properties composed of carboxyl-modified PVA, Zn $(NO_3)_2$ and $MnSO_4$.Using MnO_2 and zinc metal as cathode and anode, this electrolyte shows a higher IC of 26 mS cm^{-1}. As depicted in Fig. 12

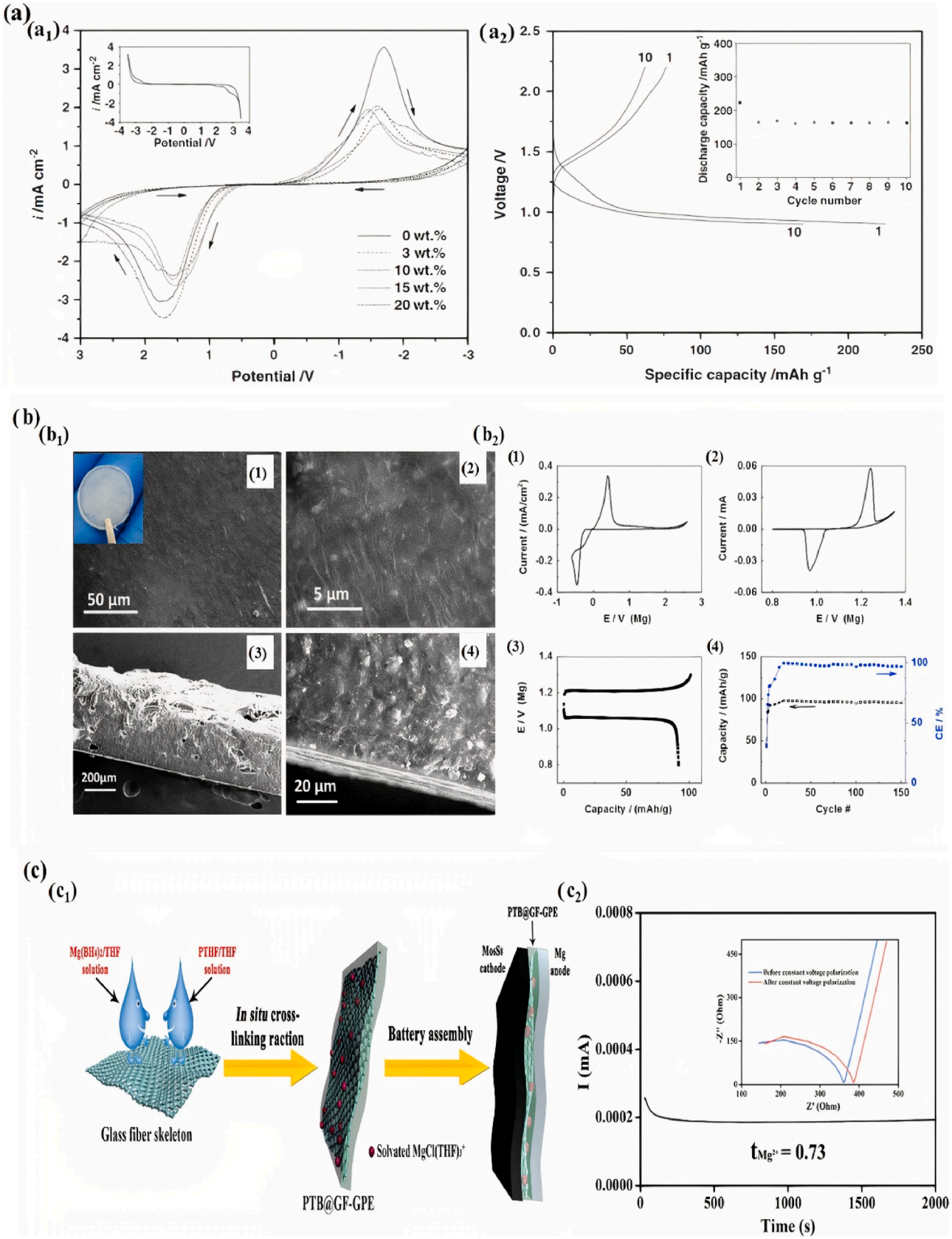

Fig. 11. **(a_1)** CV of Mg|gel nanocomposite|Mg with different amount of fumed silica, **(a_2)** Voltage vs. capacity profile of Mg-MWCNT|gel nanocomposite|MoO_3 cell [169] (Copyright 2011, Springer).**(b_1)** SEM images of the $Mg(BH_4)_2$–MgO–PEO. **(1,2)** Surface top view images. **(3,4)** Crosssectional images. **(b_2)** Electrochemical performance of $Mg(BH_4)_2$–MgO–PEO. **1)** CV (20 mVs^{-1}). **2)** CV (0.05 mVs^{-1}) of Mg intercalation/deintercalation in Mo_6S_8. **(3)** Voltage vs. capacity, **(4)** Capacity and CE vs. cycle number of a solid-state Mg cell [171] (Copyright 2015, Elsevier). **(c_1)** Schematic representation of in situ preparation of PTB@GF-GPE and the cell assembly protocol. **(c_2)** DC polarization curve of Mg//PTB@GF-GPE//Mg [172] (Copyright 2019, Wiley Online Library).

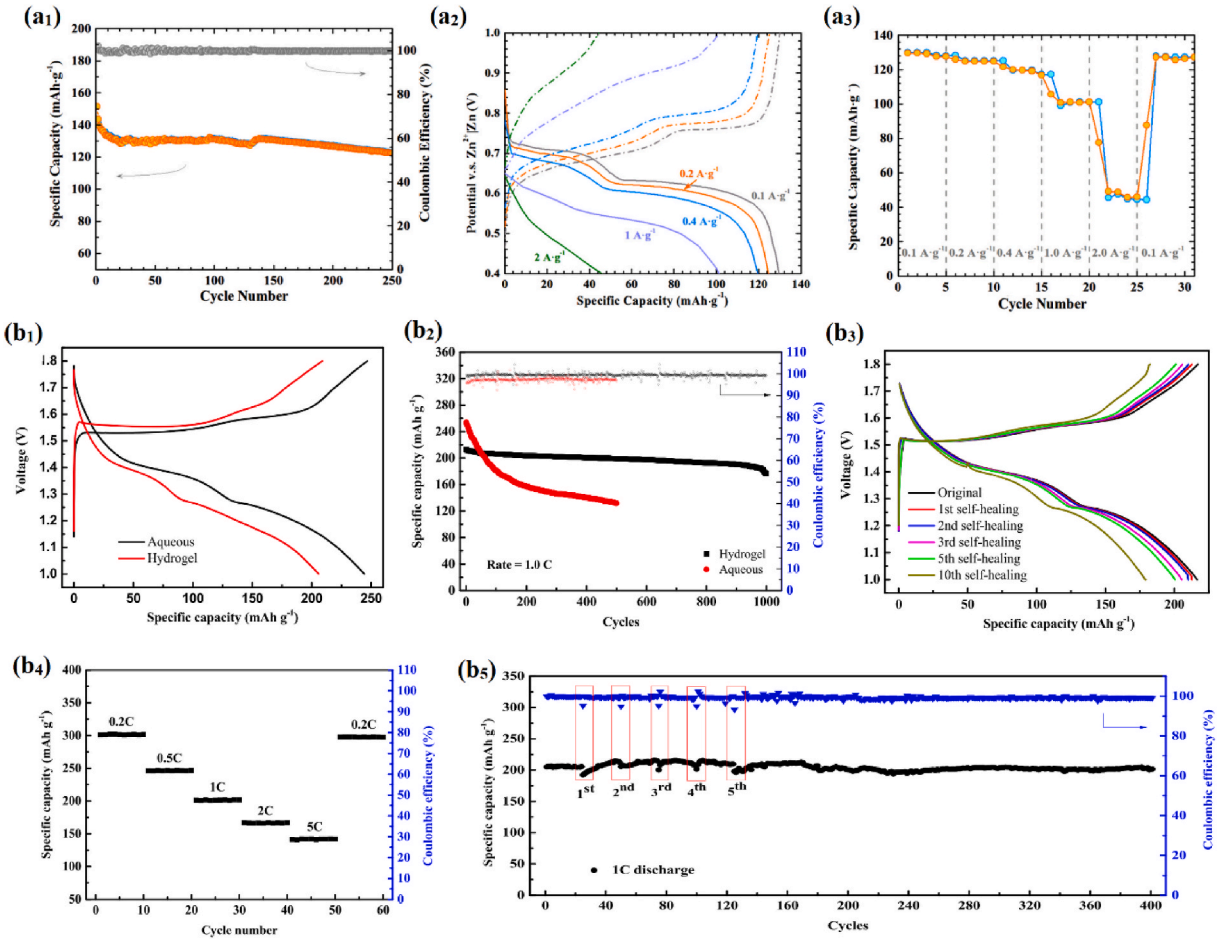

Fig. 12. **(a_1)** Specific capacity and CE vs. cycle number at 0.2 A g^{-1}, **(a_2)** Potential vs. specific capacity profile at different C-rates, **(a_3)** Rate capability capacities of the VS_2/Zn at RT [184] (Copyright 2019, Elsevier). **(b_1)** Potential vs. specific capacity curves at 1C, **(b_2)** Specific capacity and CE vs. cycle number at 1 C of the Zn//MnO_2 cells using the hydrogel and aqueous electrolytes, **(b_3)** Potential vs. specific capacity profile at 1 C, **(b_4)** Rate capability, **(b_5)** Specific capacity and CE vs. cycle number at 1C after over 5 cut/healing cycles of the QSS Zn//MnO_2 cell [188] (Copyright 2019, ACS).

b_1 and **b_2**, the aqueous battery displayed a higher reversible capacity at the initial cycles than the QSSB. However, the aqueous cell suffers from severe capacity decay and delivers only a reversible capacity of 132 mAh g ^{1} after 500 cycles with capacity retention of 52%. The full cell Zn//MnO_2 using the self-healable electrolyte exhibits a reversible capacity up to 177 mAh g ^{1} after 1000 cycles with capacity retention of 83%. Note that Zn dendrites are detected when using aqueous electrolyte. Therefore, hydrogel electrolyte prevents dendrite growth and side reactions at the electrode and electrolyte interface. As revealed in Fig. 12 b_3 and **b_5**, the reversible capacity is retained despite of several mechanical collapses, demonstrating outstanding consistency, safety, and facile maintenance, thanks to the dynamic nature of COO–Fe bond. Excellent capacity retention and excellent rate capability after 5 break/healing cycles were reported (Fig. 12 b_4). Another study reported by Mo et al. [189] on the use of polyurethane acrylate-based gel electrolyte which resists to extreme low temperatures. Good mechanical features and excellent electrochemical properties were obtained even at 20 °C (~62 mAh g ^{1} over 600 cycle). In the aim of solving safety concerns occurring during fast C-rates, the same group proposed hydrogel electrolyte composed of poly (N-isopropylacrylamide) (PNIPAM) [190].

Finally, GPE is a promising research trend which requires special attention to succeed a convenient structural design. The cross-linked structure of the gel matrix displays excellent flexibility. The preparation of a dual-network gel with a highly porous structure is the most practical method to impart excellent mechanical properties to the gel. At the same time, this structure can increase the electrolyte content and promote the migration of Zn^{2+} ions, thereby increasing the IC., the composition of the gel electrolyte should be flexibly changed. Choosing different polymer matrixes to couple with several zinc salts and modifying the charged groups through the migration of Zn^{2+} ions, which is an effective approach to improve the mobility of ions. Thus, the introduction of solutions with wide potential stability, such as organic solvents and ionic liquids, seems to be a practical method for gel electrolytes to expand the operating potential window.

7. Solid-state electrolytes for aluminum-ion batteries

A rechargeable AIB is one of the new Post-LIBs technologies of secondary batteries showing exceptional advantages, such as great abundance, safety, high theoretical gravimetric of 2980 mAh g ^{1} and volumetric capacity of 8040 mAh g ^{1} (Fig. 1). Additionally, Al can exchange 3 redox electrons per cation [191]. Nevertheless, there are still crucial issues hindering the use of this technology such as the standard redox potential of Al (1.67 V vs. SHE), which is higher than those of other metals Li (3.04 V vs. SHE) and Na (2.8 V vs. SHE), leading to a smaller working voltage. Another issue concerns the liquid electrolytes leakage and unstable interfaces produced by mechanical deformation, coupled with production of gases as well as unfavorable porous separators. For tackling these critical problems in liquid AIBs, the SSEs were introduced to highlight a novel approach for achieving high-performance energy storage AIB systems with enhanced stability

and safety. In contrast, so far there are few papers that report SSEs, more specifically polymer electrolytes, in this recent technology. So in this part we will try to explain the importance of SSEs in AIBs and leave the door open to more investigations [192,193].

Yu et al. [194] developed a new flexible solid-state AIB by placing GPE with the formulation $AlCl_3$/1-ethyl-3-methylimidazolium chloride between graphite and Al metal. This system delivered specific capacity of 120 mAh g^{-1}, 90% CE, and 91% capacity retention over 100 cycles. In addition to that, ultra-fast charge within 10s at current density of 0.6×10^{-3} A g^{-1} was demonstrated. These impressive performances were attributed to limiting mechanical deformation, aiming to stabilizing the interface between electrode and electrolyte in comparison with the liquid AIB system. Zhijing Yu et al. [192] developed a GPE composed of polyacrylamide and ionic liquid 1-ethyl-3-methylimidazolium chloride $AlCl_3$. The choice of the polymeric matrix was based on the mechanical properties, and the use of an ionic liquid serves as plasticizer to ensure good ionic percolation networks. Remarkable reversible capacity around 120 mAh g^{-1} was obtained at 60 mA g^{-1}Moreover, reversible capacity of 90 mA h g^{-1} with 95% CE was delivered over 800 cycles. This GPE formulation builds a strong interface in comparison with the liquid-based cells, efficient diffusion, and transport of chloroaluminate anions. These findings are promising for practical application for solid-sate AIBs. Isak Kim et al. [193] prepared a gel electrolyte using ethyl acrylate (EA) and $AlCl_3$/[EMIm]Cl ionic liquid. When EA is mixed in an ionic liquid with N, N′-methylene-bis-acrylamide (MBAA), which is a cross-linking agent, in an appropriate ratio, the cations and anions of the ionic liquid are accumulated in the polymer chain. These anions diffuse through electrochemical reactions at the electrode/polymer interface. They conducted several performance tests to determine the electrochemical and physicochemical properties of the developed gel polymer electrolytes. On the other hand, the full cell using the gel electrolyte exhibited enhanced performance than previous reports in terms of electrochemical cycling at high current density, and ion transport ($t_{anion} = 0.171$ at RT). It has an average reversible capacity of 85 mAh g^{-1}, with a capacity retention of almost 95% over 500 cycles, even at a high current density (200 mA g^{-1}) [192,193].

Thus, the results reported in SSEs for AIBs may possibly open a new step for low-cost and safe energy storage system that require further investigations and insights.

8. Conclusions & perspectives

Research interest for SSEs for beyond LIBs has rapidly increased. Many SSEs formulations have been reported and newly discovered in the literature. This review summarizes the similarities and differences in the chemistry and physico-chemical properties of SSEs for different battery technologies. By studying and understanding the kinetics (i.e., ionic diffusion and mechanisms), engineering efficient SSEs designs, selecting appropriate electrode materials, and proper type of SSEs will remedy safety issues and promote their use for large storage applications. We have shown throughout this review that SSEs for beyond lithium-ion batteries are generally categorized into three main groups. First, inorganic solid electrolytes, including Nasicon, metal hybrids and so on. These types of materials show high structural stability in wide range of temperature and voltage. Thus, they are considered as a potential candidate for SSEs. The three-dimensional well-ordered Nasicon type material showed a remarkably interesting ionic conductivity in the order to 10^{-3} S cm^{-1} at room temperature in the case of sodium-ion batteries. However, they are far from practical use in the case of magnesium ion batteries as they offer an ionic conductivity in the order of 10^{-5} S cm^{-1} at 400 °C and 10^{-6} S cm^{-1} at room temperature. Second category is polymer solid electrolytes which were extensively investigated as SSEs for a variety of battery technologies due to their high mechanical and shape flexibility. In one hand, solid polymers which consist of mixing a salt with a polymer exhibit good ionic conductivity at room temperature when used in sodium and magnesium-ion batteries, they have shown also interesting results in the case of zinc and calcium ion batteries. However, the low cationic transport number and high electrode–electrolyte interfacial resistance are their main drawbacks. In the other hand, gel polymers obtained through adding a salt dissolved in organic solvent into a polymer matrix could merge the high stability of solids and the diffusive properties of liquids in one electrolyte. This type of electrolytes showed an ionic conductivity close to the level of ionic conductivity of liquid electrolytes which is around 10^{-3} S cm^{-1} at room temperature for both sodium and magnesium-ion batteries. Although, concerns were raised regarding their mechanical flexibility. Last but not least, hybrid solid electrolyte were proposed to solve all the above-mentioned drawbacks. They combine the advantages of inorganic and organic materials. Higher ionic conductivity at room temperature were achieved in the case of sodium, magnesium and potassium-ion batteries which is owing to the enhanced charge transfer resistance and the electrode-electrolyte interface.

Solid-state electrolytes contribute dramatically to the battery safety enhancement and allows flexible battery architectures. However, the poor contact with isolated particles of the active material, the volume variations, the low ionic conductivity, and poor interfacial contact with electrodes remains unresolved in literature. In fact, the approaches adopted in the case of Na- and K-ion batteries are mostly similar to the ones reported for Li-ion batteries. However, for multivalent systems such as Ca-, Mg and Al-batteries, the multivalent ions with large ionic radii and high charges are vulnerable to interact with an energetic/steric trap, which hinders the migration of ions. In addition to that, the native oxide layer present on the metals surface: CaO, MgO and Al_2O_3 for Ca, Mg and Al respectively, hinders the reversible plating/stripping on the metal and requires continuous removal to create activated sites for plating/stripping.

Furthermore, this review lists the important parameters, comprising cycling stability, rate capability, IC, cell configuration, E_a, flexibility and electrolyte of recent research works involved SSEs for beyond LIBs. For instance, the current reported IC is still very low which hinders the development of high-rate and high-power density all-solid-state batteries. Therefore, controlling and enhancing all the parameters would contribute to accomplish better battery performance for several applications, from grid to mobile applications while ensuring high safety. It is expected that demonstration for SSBs as rechargeable batteries at the industrial level could start soon even though we still face many tough challenges. Thus, the results reported in this review may open a new step for low-cost and safe energy storage systems that require further investigations. Moreover, since that under the operating conditions of all-solid-state batteries, the SSEs must be entirely compatible with Li metal, chemically and electrochemically stable. Unfortunately, several SSE polymers, hybrid and inorganic materials are not thermodynamically stable against Li metal and/or experience phase change during cycling. It is critical to push further into these challenges and locate good alternatives such as SSE technologies for beyond LIBs. Owing to their higher compromise between stability and electrochemical performance, these solid-state batteries beyond lithium, as aforementioned, seem have better practical applications and potentials. Nevertheless, in-depth investigations are required to further understanding including mechanisms of alkali and alkaline earth metal mobility into the SSEs, in-situ and operando electrode/electrolyte interface studies, structural and compositional investigations, theoretical calculations, safety studies using nails penetration under extreme conditions and the scalability of these technologies.

Funding

This research did not receive any specific grant from funding agencies in the public, commercial, or not-for-profit sectors.

Author contributions

Dr Hasna AZIAM: Writing of the section dedicated to Sodium-ion batteries **Mr Badre LARHRIB:** Writing of the section dedicated to Potassium/ Zinc/ Aluminum-ion batteries **Dr Noha SABI**: Writing of the section dedicated to Calcium-ion batteries **Mrs Charifa HAKIM**: Writing of the section dedicated to Magnesium-ion batteries **Prof Hicham BEN YOUCEF:** Co-supervising, Writing of the sections related to Polymer & Composite electrolytes **Prof Ismael SAADOUNE**: Supervising, Writing, Review & Editing, Polishing.

Declaration of competing interest

The authors declare that they have no known competing financial interests or personal relationships that could have appeared to influence the work reported in this paper.

Data availability

The authors are unable or have chosen not to specify which data has been used.

References

[1] Che H, Chen S, Xie Y, Wang H, Amine K, Liao X-Z, Ma Z-F. Electrolyte design strategies and research progress for room-temperature sodium-ion batteries. Energy Environ Sci 2017;10:1075–101. https://doi.org/10.1039/C7EE00524E.

[2] Gao Y, Chen G, Wang X, Yang H, Wang Z, Lin W, Xu H, Bai Y, Wu C. PY13FSI-infiltrated SBA-15 as nonflammable and high ion-conductive ionogel electrolytes for quasi-solid-state sodium-ion batteries. ACS Appl Mater Interfaces 2020;12:22981–91. https://doi.org/10.1021/acsami.0c04878.

[3] Blomgren GE. Liquid electrolytes for lithium and lithium-ion batteries. J Power Sources 2003;119–121:326–9. https://doi.org/10.1016/S0378-7753(03)00147-2.

[4] Chen J, Wu J, Wang X, Zhou A, Yang Z. Research progress and application prospect of solid-state electrolytes in commercial lithium-ion power batteries. Energy Storage Mater 2021;35:70–87. https://doi.org/10.1016/j.ensm.2020.11.017.

[5] Du G, Tao M, Li J, Yang T, Gao W, Deng J, Qi Y, Bao S, Xu M. Low-operating temperature, high-rate and durable solid-state sodium-ion battery based on polymer electrolyte and prussian blue cathode. Adv Energy Mater 2020;10:1903351. https://doi.org/10.1002/aenm.201903351.

[6] Zhang D, Cao X, Xu D, Wang N, Yu C, Hu W, Yan X, Mi J, Wen B, Wang L, Zhang L. Synthesis of cubic Na3SbS4 solid electrolyte with enhanced ion transport for all-solid-state sodium-ion batteries. Electrochim Acta 2018;259:100–9. https://doi.org/10.1016/j.electacta.2017.10.173.

[7] Zhang Y, Wu Y, Liu Y, Feng J. Flexible and freestanding heterostructures based on COF-derived N-doped porous carbon and two-dimensional MXene for all-solid-state lithium-sulfur batteries. Chem Eng J 2022;428:131040. https://doi.org/10.1016/j.cej.2021.131040.

[8] Huang J, Liang F, Hou M, Zhang Y, Chen K, Xue D. Garnet-type solid-state electrolytes and interfaces in all-solid-state lithium batteries: progress and perspective. Appl Mater Today 2020;20:100750. https://doi.org/10.1016/j.apmt.2020.100750.

[9] Ding W-Q, Lv F, Xu N, Wu M-T, Liu J, Gao X-P. Polyethylene oxide-based solid-state composite polymer electrolytes for rechargeable lithium batteries. ACS Appl Energy Mater 2021;4:4581–601. https://doi.org/10.1021/acsaem.1c00216.

[10] Mezzomo L, Bonato S, Mostoni S, Credico BD, Scotti R, D'Arienzo M, Mustarelli P, Ruffo R. Composite solid-state electrolyte based on hybrid poly(ethylene glycol)-silica fillers enabling long-life lithium metal batteries. Electrochim Acta 2022;411:140060. https://doi.org/10.1016/j.electacta.2022.140060.

[11] Zhang H, Chen Y, Li C, Armand M. Electrolyte and anode-electrolyte interphase in solid-state lithium metal polymer batteries: a perspective. SusMat 2021;1:24–37. https://doi.org/10.1002/sus2.6.

[12] Gurung A, Pokharel J, Baniya A, Pathak R, Chen K, Lamsal BS, Ghimire N, Zhang W-H, Zhou Y, Qiao Q. A review on strategies addressing interface incompatibilities in inorganic all-solid-state lithium batteries. Sustain Energy Fuels 2019;3:3279–309. https://doi.org/10.1039/C9SE00549H.

[13] Zhao W, Yi J, He P, Zhou H. Solid-state electrolytes for lithium-ion batteries: fundamentals, challenges and perspectives. Electrochem. Energ. Rev. 2019;2:574–605. https://doi.org/10.1007/s41918-019-00048-0.

[14] Zheng Y, Yao Y, Ou J, Li M, Luo D, Dou H, Li Z, Amine K, Yu A, Chen Z. A review of composite solid-state electrolytes for lithium batteries: fundamentals, key materials and advanced structures. Chem Soc Rev 2020;49:8790–839. https://doi.org/10.1039/D0CS00305K.

[15] Shanmukaraj D, Ranque P, Youcef HB, Rojo T, Poizot P, Grugeon S, Laruelle S, Guyomard D. Review—towards efficient energy storage materials: lithium intercalation/organic electrodes to polymer electrolytes—a road map (tribute to michel armand). J Electrochem Soc 2020;167:070530. https://doi.org/10.1149/1945-7111/ab787a.

[16] Armand M. Polymer solid electrolytes - an overview. Solid State Ionics 1983;9–10:745–54. https://doi.org/10.1016/0167-2738(83)90083-8.

[17] Armand MB, Duclot MJ, Rigaud Ph. Polymer solid electrolytes: stability domain. Solid State Ionics 1981;3–4:429–30. https://doi.org/10.1016/0167-2738(81)90126-0.

[18] Ye F, Liao K, Ran R, Shao Z. Recent advances in filler engineering of polymer electrolytes for solid-state Li-ion batteries: a review. Energy Fuels 2020;34:9189–207. https://doi.org/10.1021/acs.energyfuels.0c02111.

[19] Zaman W, Hatzell KB. Processing and manufacturing of next generation lithium-based all solid-state batteries. Curr Opin Solid State Mater Sci 2022;26:101003. https://doi.org/10.1016/j.cossms.2022.101003.

[20] Grosjean C, Miranda PH, Perrin M, Poggi P. Assessment of world lithium resources and consequences of their geographic distribution on the expected development of the electric vehicle industry. Renew Sustain Energy Rev 2012;16:1735–44. https://doi.org/10.1016/j.rser.2011.11.023.

[21] Chen L, An Q, Mai L. Recent advances and prospects of cathode materials for rechargeable aqueous zinc-ion batteries. Adv Mater Interfac 2019;6:1900387. https://doi.org/10.1002/admi.201900387.

[22] Jia H, Wang Z, Tawiah B, Wang Y, Chan C-Y, Fei B, Pan F. Recent advances in zinc anodes for high-performance aqueous Zn-ion batteries. Nano Energy 2020;70:104523. https://doi.org/10.1016/j.nanoen.2020.104523.

[23] Chu I-H, Kompella CS, Nguyen H, Zhu Z, Hy S, Deng Z, Meng YS, Ong SP. Room-temperature all-solid-state rechargeable sodium-ion batteries with a Cl-doped Na_3PS_4 superionic conductor. Sci Rep 2016;6:33733. https://doi.org/10.1038/srep33733.

[24] Hayashi A, Masuzawa N, Yubuchi S, Tsuji F, Hotehama C, Sakuda A, Tatsumisago M. A sodium-ion sulfide solid electrolyte with unprecedented conductivity at room temperature. Nat Commun 2019;10:5266. https://doi.org/10.1038/s41467-019-13178-2.

[25] Xie D, Zhang M, Wu Y, Xiang L, Tang Y. A flexible dual-ion battery based on sodium-ion quasi-solid-state electrolyte with long cycling life. Adv Funct Mater 2020;30:1906770. https://doi.org/10.1002/adfm.201906770.

[26] Ramos EP, Zhang Z, Assoud A, Kaup K, Lalère F, Nazar LF. Correlating ion mobility and single crystal structure in sodium-ion chalcogenide-based solid state fast ion conductors: Na11Sn2PnS12 (pn = Sb, P). Chem Mater 2018;30:7413–7. https://doi.org/10.1021/acs.chemmater.8b02077.

[27] Hayashi A, Noi K, Sakuda A, Tatsumisago M. Superionic glass-ceramic electrolytes for room-temperature rechargeable sodium batteries. Nat Commun 2012;3:856. https://doi.org/10.1038/ncomms1843.

[28] Hayashi A, Noi K, Tanibata N, Nagao M, Tatsumisago M. High sodium ion conductivity of glass–ceramic electrolytes with cubic Na_3PS_4. J Power Sources 2014;258:420–3. https://doi.org/10.1016/j.jpowsour.2014.02.054.

[29] Wenzel S, Leichtweiss T, Weber DA, Sann J, Zeier WG, Janek J. Interfacial reactivity benchmarking of the sodium ion conductors Na_3PS_4 and sodium β-alumina for protected sodium metal anodes and sodium all-solid-state batteries. ACS Appl Mater Interfaces 2016;8:28216–24. https://doi.org/10.1021/acsami.6b10119.

[30] Zhang D, Cao X, Xu D, Wang N, Yu C, Hu W, Yan X, Mi J, Wen B, Wang L, Zhang L. Synthesis of cubic Na3SbS4 solid electrolyte with enhanced ion transport for all-solid-state sodium-ion batteries. Electrochim Acta 2018;259:100–9. https://doi.org/10.1016/j.electacta.2017.10.173.

[31] Yu Z, Shang S, Seo J, Wang D, Luo X, Huang Q, Chen S, Lu J, Li X, Liu Z, Wang D. Exceptionally high ionic conductivity in $Na_3P_{0.62}As_{0.38}S_4$ with improved moisture stability for solid-state sodium-ion batteries. Adv Mater 2017;29:1605561. https://doi.org/10.1002/adma.201605561.

[32] Banerjee A, Park KH, Heo JW, Nam YJ, Moon CK, Oh SM, Hong S-T, Jung YS. Na_3SbS_4 : a solution processable sodium superionic conductor for all-solid-state sodium-ion batteries. Angew Chem 2016;128:9786–90. https://doi.org/10.1002/ange.201604158.

[33] Duchêne L, Kühnel R-S, Stilp E, Cuervo Reyes E, Remhof A, Hagemann H, et al. A stable 3 V all-solid-state sodium–ion battery based on a *closo* -borate electrolyte. Energy Environ Sci 2017;10:2609–15. https://doi.org/10.1039/C7EE02420G.

[34] Lalère F, Leriche JB, Courty M, Boulineau S, Viallet V, Masquelier C, Seznec V. An all-solid state NASICON sodium battery operating at 200 °C. J Power Sources 2014;247:975–80. https://doi.org/10.1016/j.jpowsour.2013.09.051.

[35] Guin M, Tietz F, Guillon O. New promising NASICON material as solid electrolyte for sodium-ion batteries: correlation between composition, crystal structure and ionic conductivity of Na3+xSc2SixP3 xO12. Solid State Ionics 2016;293:18–26. https://doi.org/10.1016/j.ssi.2016.06.005.

[36] de la Torre-Gamarra C, Appetecchi GB, Ulissi U, Varzi A, Varez A, Passerini S. Na3Si2Y0.16Zr1.84PO12-ionic liquid hybrid electrolytes: an approach for realizing solid-state sodium-ion batteries? J Power Sources 2018;383:157–63. https://doi.org/10.1016/j.jpowsour.2017.12.037.

[37] Evstigneeva MA, Nalbandyan VB, Petrenko AA, Medvedev BS, Kataev AA. A new family of fast sodium ion conductors: Na2M2TeO6 (M = Ni, Co, Zn, Mg). Chem Mater 2011;23:1174–81. https://doi.org/10.1021/cm102629g.

[38] Li et al. - 2018 - A P2-type layered superionic conductor Ga-doped Na.pdf, (n.d.)..

[39] Zhao Y, Liu Z, Xu J, Zhang T, Zhang F, Zhang X. Synthesis and characterization of a new perovskite-type solid-state electrolyte of Na1/3La1/3Sr1/3ZrO3 for all-solid-state sodium-ion batteries. J Alloys Compd 2019;783:219–25. https://doi.org/10.1016/j.jallcom.2018.12.289.

[40] Amores M, Baker PJ, Cussen EJ, Corr SA. Na 1.5 La 1.5 TeO 6 : Na + conduction in a novel Na-rich double perovskite. Chem Commun 2018;54:10040–3. https://doi.org/10.1039/C8CC03367F.

[41] Yang FZT, Peterson VK, Schmid S. Composition and temperature dependent structural investigation of the perovskite-type sodium-ion solid electrolyte series Na1/2 xLa1/2 xSr2xZrO3. J Alloys Compd 2021;863:158500. https://doi.org/10.1016/j.jallcom.2020.158500.

[42] Yang YQ, Chang Z, Li MX, Wang XW, Wu YP. A sodium ion conducting gel polymer electrolyte. Solid State Ionics 2015;269:1–7. https://doi.org/10.1016/j.ssi.2014.11.015.

[43] Guo J-Z, Yang A-B, Gu Z-Y, Wu X-L, Pang W-L, Ning Q-L, Li W-H, Zhang J-P, Su Z-M. Quasi-solid-state sodium-ion full battery with high-power/energy densities. ACS Appl Mater Interfaces 2018;10:17903–10. https://doi.org/10.1021/acsami.8b02768.

[44] Zhu X, Zhao R, Deng W, Ai X, Yang H, Cao Y. An all-solid-state and all-organic sodium-ion battery based on redox-active polymers and plastic crystal electrolyte. Electrochim Acta 2015;178:55–9. https://doi.org/10.1016/j.electacta.2015.07.163.

[45] Yang J, Zhang H, Zhou Q, Qu H, Dong T, Zhang M, Tang B, Zhang J, Cui G. Safety-enhanced polymer electrolytes for sodium batteries: recent progress and perspectives. ACS Appl Mater Interfaces 2019;11:17109–27. https://doi.org/10.1021/acsami.9b01239.

[46] Gebert F, Knott J, Gorkin R, Chou S-L, Dou S-X. Polymer electrolytes for sodium-ion batteries. Energy Storage Mater 2021;36:10–30. https://doi.org/10.1016/j.ensm.2020.11.030.

[47] Bhargav PB, Mohan VM, Sharma AK, Rao VVRN. Investigations on electrical properties of (PVA:NaF) polymer electrolytes for electrochemical cell applications. Curr Appl Phys 2009;9:165–71. https://doi.org/10.1016/j.cap.2008.01.006.

[48] Polu AR, Kumar R. Preparation and characterization of pva based solid polymer electrolytes for electrochemical cell applications. Chin J Polym Sci 2013;31:641–8. https://doi.org/10.1007/s10118-013-1246-3.

[49] Duraikkan V, Sultan AB, Nallaperumal N, Shunmuganarayanan A. Structural, thermal and electrical properties of polyvinyl alcohol/poly(vinyl pyrrolidone)–sodium nitrate solid polymer blend electrolyte. Ionics 2018;24:139–51. https://doi.org/10.1007/s11581-017-2169-8.

[50] Aziz SB, Abdullah OGh, Rasheed MA. Structural and electrical characteristics of PVA:NaTf based solid polymer electrolytes: role of lattice energy of salts on electrical DC conductivity. J Mater Sci Mater Electron 2017;28:12873–84. https://doi.org/10.1007/s10854-017-7117-x.

[51] Farah N, Ng HM, Numan A, Liew C-W, Latip NAA, Ramesh K, Ramesh S. Solid polymer electrolytes based on poly(vinyl alcohol) incorporated with sodium salt and ionic liquid for electrical double layer capacitor. Mater Sci Eng, B 2019;251:114468. https://doi.org/10.1016/j.mseb.2019.114468.

[52] Osman Z, Isa KBM, Othman L, Kamarulzaman N. Studies of ionic conductivity and dielectric behavior in polyacrylonitrile based solid polymer electrolytes. Defect Diffusion Forum 2011;312–315:116–21. https://doi.org/10.4028/www.scientific.net/DDF.312-315.116.

[53] Vignarooban K, Badami P, Dissanayake MAKL, Ravirajan P, Kannan AM. Poly-acrylonitrile-based gel-polymer electrolytes for sodium-ion batteries. Ionics 2017;23:2817–22. https://doi.org/10.1007/s11581-017-2002-4.

[54] Sångeland C, Mogensen R, Brandell D, Mindemark J. Stable cycling of sodium metal all-solid-state batteries with polycarbonate-based polymer electrolytes. ACS Appl. Polym. Mater. 2019;1:825–32. https://doi.org/10.1021/acsapm.9b00068.

[55] Venkata Subba Rao C, Ravi M, Raja V, Balaji Bhargav P, Sharma AK, Narasimha Rao VVR. Preparation and characterization of PVP-based polymer electrolytes for solid-state battery applications. Iran Polym J (Engl Ed) 2012;21:531–6. https://doi.org/10.1007/s13726-012-0058-6.

[56] Karpagavel K, Sundaramahalingam K, Manikandan A, Vanitha D, Manohar A, Nagarajan ER, Nallamuthu N. Electrical properties of lithium-ion conducting poly (vinylidene fluoride-Co-hexafluoropropylene) (PVDF-HFP)/Polyvinylpyrrolidone (PVP) solid polymer electrolyte. J Electron Mater 2021;50:4415–25. https://doi.org/10.1007/s11664-021-08967-9.

[57] Koduru HK, Scarpelli F, Marinov YG, Hadjichristov GB, Rafailov PM, Miloushev IK, Petrov AG, Godbert N, Bruno L, Scaramuzza N. Characterization of PEO/PVP/GO nanocomposite solid polymer electrolyte membranes: microstructural, thermo-mechanical, and conductivity properties. Ionics 2018;24:3459–73. https://doi.org/10.1007/s11581-018-2484-8.

[58] Sadiq M, Raza MMH, Murtaza T, Zulfequar M, Ali J. Sodium ion-conducting polyvinylpyrrolidone (PVP)/Polyvinyl alcohol (PVA) blend electrolyte films. J Electron Mater 2021;50:403–18. https://doi.org/10.1007/s11664-020-08581-1.

[59] Vahini M, Muthuvinayagam M. Synthesis and electrochemical studies on sodium ion conducting PVP based solid polymer electrolytes. J Mater Sci Mater Electron 2019;30:5609–19. https://doi.org/10.1007/s10854-019-00854-8.

[60] Zhang X, Wang X, Liu S, Tao Z, Chen J. A novel PMA/PEG-based composite polymer electrolyte for all-solid-state sodium ion batteries. Nano Res 2018;11:6244–51. https://doi.org/10.1007/s12274-018-2144-3.

[61] Efficient gel-polymer electrolyte for sodium-ion batteries based on poly (acrylonitrile-co-methyl acrylate). Electrochim Acta 2020;334:135512. https://doi.org/10.1016/j.electacta.2019.135512.

[62] Ion transport and ion–filler-polymer interaction in poly(methyl methacrylate)-based, sodium ion conducting, gel polymer electrolytes dispersed with silica nanoparticles. J Power Sources 2010;195:5101–8. https://doi.org/10.1016/j.jpowsour.2010.02.026.

[63] Qi X, Ma Q, Liu L, Hu Y-S, Li H, Zhou Z, Huang X, Chen L. Sodium bis (fluorosulfonyl)imide/poly(ethylene oxide) polymer electrolytes for sodium-ion batteries. Chemelectrochem 2016;3:1741–5. https://doi.org/10.1002/celc.201600221.

[64] Colò F, Bella F, Nair JR, Gerbaldi C. Light-cured polymer electrolytes for safe, low-cost and sustainable sodium-ion batteries. J Power Sources 2017;365:293–302. https://doi.org/10.1016/j.jpowsour.2017.08.079.

[65] Chen S, Feng F, Yin Y, Lizo X, Ma Z. Plastic crystal polymer electrolytes containing boron based anion acceptors for room temperature all-solid-state sodium-ion batteries. Energy Storage Mater 2019;22:57–65. https://doi.org/10.1016/j.ensm.2018.12.023.

[66] Gao W, Du G, Qi Y, Yang Q, Du W, Xu M. Na $_2$ TiV (PO $_4$) $_3$ @C composite with excellent Na-storage performance based on a solid-state polymer electrolyte membrane. Int J Energy Res 2021;45:8008–17. https://doi.org/10.1002/er.6303.

[67] West K, Zachau-Christiansen B, Jacobsen T, Hiort-Lorenzen E, Skaarup S. Poly (ethylene oxide)-sodium perchlorate electrolytes in solid-state sodium cells. Br Polym J 1988;20:243–6. https://doi.org/10.1002/pi.4980200315.

[68] Hashmi SA, Chandra S. Experimental investigations on a sodium-ion-conducting polymer electrolyte based on poly(ethylene oxide) complexed with NaPF6. Mater Sci Eng, B 1995;34:18–26. https://doi.org/10.1016/0921-5107(95)01219-2.

[69] Chandrasekaran R, Selladurai S. Preparation and characterization of a new polymer electrolyte (PEO:NaClO3) for battery application. J Solid State Electrochem 2001;5:355–61. https://doi.org/10.1007/s100080000156.

[70] Boschin A, Johansson P. Characterization of NaX (X: TFSI, FSI) – PEO based solid polymer electrolytes for sodium batteries. Electrochim Acta 2015;175:124–33. https://doi.org/10.1016/j.electacta.2015.03.228.

[71] Ni'mah YL, Cheng M-Y, Cheng JH, Rick J, Hwang B-J. Solid-state polymer nanocomposite electrolyte of TiO2/PEO/NaClO4 for sodium ion batteries. J Power Sources 2015;278:375–81. https://doi.org/10.1016/j.jpowsour.2014.11.047.

[72] Colò F, Bella F, Nair JR, Destro M, Gerbaldi C. Cellulose-based novel hybrid polymer electrolytes for green and efficient Na-ion batteries. Electrochim Acta 2015;174:185–90. https://doi.org/10.1016/j.electacta.2015.05.178.

[73] Bhargav PB, Mohan VM, Sharma AK, Rao VVRN. Characterization of poly(vinyl alcohol)/sodium bromide polymer electrolytes for electrochemical cell applications. J Appl Polym Sci 2008;108:510–7. https://doi.org/10.1002/app.27566.

[74] Osman Z, Md Isa KB, Ahmad A, Othman L. A comparative study of lithium and sodium salts in PAN-based ion conducting polymer electrolytes. Ionics 2010;16:431–5. https://doi.org/10.1007/s11581-009-0410-9.

[75] Naresh Kumar K, Sreekanth T, Jaipal Reddy M, Subba Rao UV. Study of transport and electrochemical cell characteristics of PVP:NaClO3 polymer electrolyte system. J Power Sources 2001;101:130–3. https://doi.org/10.1016/S0378-7753(01)00658-9.

[76] Kiran Kumar K, Ravi M, Pavani Y, Bhavani S, Sharma AK, Narasimha Rao VVR. Investigations on the effect of complexation of NaF salt with polymer blend (PEO/PVP) electrolytes on ionic conductivity and optical energy band gaps. Phys B Condens Matter 2011;406:1706–12. https://doi.org/10.1016/j.physb.2011.02.010.

[77] Cheng M, Qu T, Zi J, Yao Y, Liang F, Ma W, Yang B, Dai Y, Lei Y. A hybrid solid electrolyte for solid-state sodium ion batteries with good cycle performance. Nanotechnology 2020;31:425401. https://doi.org/10.1088/1361-6528/aba059.

[78] Chen G, Ye L, Zhang K, Gao M, Lu H, Xu H, Bai Y, Wu C. Hyperbranched polyether boosting ionic conductivity of polymer electrolytes for all-solid-state sodium ion batteries. Chem Eng J 2020;394:124885. https://doi.org/10.1016/j.cej.2020.124885.

[79] Eftekhari A. Potassium secondary cell based on Prussian blue cathode. J Power Sources 2004;126:221–8. https://doi.org/10.1016/j.jpowsour.2003.08.007.

[80] M. Waki, K. Miyamoto, K. Aoki, (54) manufacturing method of, (n.d.) 13.

[81] Komaba S, Hasegawa T, Dahbi M, Kubota K. Potassium intercalation into graphite to realize high-voltage/high-power potassium-ion batteries and potassium-ion capacitors. Electrochem Commun 2015;60:172–5. https://doi.org/10.1016/j.elecom.2015.09.002.

[82] Caracciolo L, Madec L, Gachot G, Martinez H. Impact of the salt anion on K metal reactivity in EC/DEC studied using GC and XPS analysis. ACS Appl Mater Interfaces 2021;13:57505–13. https://doi.org/10.1021/acsami.1c19537.

[83] Du G, Tao M, Liu D, Aslam MK, Qi Y, Jiang J, Li Y, Bao S, Xu M. Low-operating temperature quasi-solid-state potassium-ion battery based on commercial materials. J Colloid Interface Sci 2021;582:932–9. https://doi.org/10.1016/j.jcis.2020.08.069.

[84] Liu H, Cheng X-B, Huang J-Q, Yuan H, Lu Y, Yan C, Zhu G-L, Xu R, Zhao C-Z, Hou L-P, He C, Kaskel S, Zhang Q. Controlling dendrite growth in solid-state electrolytes. ACS Energy Lett 2020;5:833–43. https://doi.org/10.1021/acsenergylett.9b02660.

[85] Rajagopalan R, Tang Y, Ji X, Jia C, Wang H. Advancements and challenges in potassium ion batteries: a comprehensive review. Adv Funct Mater 2020;30:1909486. https://doi.org/10.1002/adfm.201909486.

[86] Fei H, Liu Y, An Y, Xu X, Zeng G, Tian Y, Ci L, Xi B, Xiong S, Feng J. Stable all-solid-state potassium battery operating at room temperature with a composite polymer electrolyte and a sustainable organic cathode. J Power Sources 2018;399:294–8. https://doi.org/10.1016/j.jpowsour.2018.07.124.

[87] Fei H, Liu Y, An Y, Xu X, Zhang J, Xi B, Xiong S, Feng J. Safe all-solid-state potassium batteries with three dimensional, flexible and binder-free metal sulfide array electrode. J Power Sources 2019;433:226697. https://doi.org/10.1016/j.jpowsour.2019.226697.

[88] Hu Z, Liu Q, Chou S-L, Dou S-X. Advances and challenges in metal sulfides/selenides for next-generation rechargeable sodium-ion batteries. Adv Mater 2017;29:1700606. https://doi.org/10.1002/adma.201700606.

[89] Yuan H, Li H, Zhang T, Li G, He T, Du F, Feng S. A K2Fe4O7 superionic conductor for all-solid-state potassium metal batteries. J Mater Chem A 2018;6:8413–8. https://doi.org/10.1039/C8TA01418C.

[90] Doux J-M, Leguay L, Le Gal La Salle A, Joubert O, Quarez E. K3Sb4O10(BO3): a solid state K-ion conductor. Solid State Ionics 2018;324:260–6. https://doi.org/10.1016/j.ssi.2018.07.018.

[91] Lu K, Zhang H, Gao S, Cheng Y, Ma H. High rate and stable symmetric potassium ion batteries fabricated with flexible electrodes and solid-state electrolytes. Nanoscale 2018;10:20754–60. https://doi.org/10.1039/C8NR07268J.

[92] Xiao R, Li H, Chen L. High-throughput computational discovery of K2CdO2 as an ion conductor for solid-state potassium-ion batteries. J Mater Chem A 2020;8:5157–62. https://doi.org/10.1039/C9TA13105A.

[93] Zheng J, Fang H, Fan L, Ren Y, Jena P, Wu Y. Antiperovskite K3OI for K-ion solid state electrolyte. J Phys Chem Lett 2021;12:7120–6. https://doi.org/10.1021/acs.jpclett.1c01807.

[94] Haffner A, Hatz A-K, Zeman OEO, Hoch C, Lotsch BV, Johrendt D. Polymorphism and fast potassium-ion conduction in the T5 supertetrahedral phosphidosilicate KSi2P3. Angew Chem Int Ed 2021;60:13641–6. https://doi.org/10.1002/anie.202101187.

[95] Arroyo-de Dompablo ME, Ponrouch A, Johansson P, Palacín MR. Achievements, challenges, and prospects of calcium batteries. Chem Rev 2020;120:6331–57. https://doi.org/10.1021/acs.chemrev.9b00339.

[96] Stievano L, de Meatza I, Bitenc J, Cavallo C, Brutti S, Navarra MA. Emerging calcium batteries. J Power Sources 2021;482:228875. https://doi.org/10.1016/j.jpowsour.2020.228875.

[97] Poizot P, Dolhem F, Gaubicher J. Progress in all-organic rechargeable batteries using cationic and anionic configurations: toward low-cost and greener storage solutions? Curr Opin Electrochem 2018;9:70–80. https://doi.org/10.1016/j.coelec.2018.04.003.

[98] Hosein ID. The promise of calcium batteries: open perspectives and fair comparisons. ACS Energy Lett 2021;6:1560–5. https://doi.org/10.1021/acsenergylett.1c00593.

[99] Aurbach D, Skaletsky R, Gofer Y. The electrochemical behavior of calcium electrodes in a few organic electrolytes. J Electrochem Soc 1991;138:3536. https://doi.org/10.1149/1.2085455.

[100] See KA, Gerbec JA, Jun Y-S, Wudl F, Stucky GD, Seshadri R. A high capacity calcium primary cell based on the Ca–S system. Adv Energy Mater 2013;3:1056–61. https://doi.org/10.1002/aenm.201300160.

[101] Kim H, Boysen DA, Bradwell DJ, Chung B, Jiang K, Tomaszowska AA, Wang K, Wei W, Sadoway DR. Thermodynamic properties of calcium–bismuth alloys determined by emf measurements. Electrochim Acta 2012;60:154–62. https://doi.org/10.1016/j.electacta.2011.11.023.

[102] Newhouse JM, Poizeau S, Kim H, Spatocco BL, Sadoway DR. Thermodynamic properties of calcium–magnesium alloys determined by emf measurements. Electrochim Acta 2013;91:293–301. https://doi.org/10.1016/j.electacta.2012.11.063.

[103] Poizeau S, Kim H, Newhouse JM, Spatocco BL, Sadoway DR. Determination and modeling of the thermodynamic properties of liquid calcium–antimony alloys. Electrochim Acta 2012;76:8–15. https://doi.org/10.1016/j.electacta.2012.04.139.

[104] Lu Z, Ciucci F. Metal borohydrides as electrolytes for solid-state Li, Na, Mg, and Ca batteries: a first-principles study. Chem Mater 2017;29:9308–19. https://doi.org/10.1021/acs.chemmater.7b03284.

[105] Genier FS, Burdin CV, Biria S, Hosein ID. A novel calcium-ion solid polymer electrolyte based on crosslinked poly(ethylene glycol) diacrylate. J Power Sources 2019;414:302–7. https://doi.org/10.1016/j.jpowsour.2019.01.017.

[106] Wang J, Genier FS, Li H, Biria S, Hosein ID. A solid polymer electrolyte from cross-linked polytetrahydrofuran for calcium ion conduction. ACS Appl. Polym. Mater. 2019;1:1837–44. https://doi.org/10.1021/acsapm.9b00371.

[107] Martinez-Cisneros CS, Fernandez A, Antonelli C, Levenfeld B, Varez A, Vezzù K, Di Noto V, Sanchez J-Y. Opening the door to liquid-free polymer electrolytes for calcium batteries. Electrochim Acta 2020;353:136525. https://doi.org/10.1016/j.electacta.2020.136525.

[108] Koettgen J, Bartel CJ, Shen J-X, Persson KA, Ceder G. First-principles study of CaB12H12 as a potential solid-state conductor for Ca. Phys Chem Chem Phys 2020;22:27600–4. https://doi.org/10.1039/D0CP04500D.

[109] Aurbach D, Gofer Y, Lu Z, Schechter A, Chusid O, Gizbar H, Cohen Y, Ashkenazi V, Moshkovich M, Turgeman R. A short review on the comparison between Li battery systems and rechargeable magnesium battery technology. J Power Sources 2001;97–98:28–32. https://doi.org/10.1016/S0378-7753(01)00585-7.

[110] Massé RC, Uchaker E, Cao G. Beyond Li-ion: electrode materials for sodium- and magnesium-ion batteries. Sci. China Mater. 2015;58:715–66. https://doi.org/10.1007/s40843-015-0084-8.

[111] Huie MM, Bock DC, Takeuchi ES, Marschilok AC, Takeuchi KJ. Cathode materials for magnesium and magnesium-ion based batteries. Coord Chem Rev 2015;287:15–27. https://doi.org/10.1016/j.ccr.2014.11.005.

[112] Lu Z, Schechter A, Moshkovich M, Aurbach D. On the electrochemical behavior of magnesium electrodes in polar aprotic electrolyte solutions. J Electroanal Chem 1999;466:203–17. https://doi.org/10.1016/S0022-0728(99)00146-1.

[113] Muldoon J, Bucur CB, Oliver AG, Sugimoto T, Matsui M, Kim HS, Allred GD, Zajicek J, Kotani Y. Electrolyte roadblocks to a magnesium rechargeable battery. Energy Environ Sci 2012;5:5941–50. https://doi.org/10.1039/c2ee03029b.

[114] Song J, Sahadeo E, Noked M, Lee SB. Mapping the challenges of magnesium battery. J Phys Chem Lett 2016;7:1736–49. https://doi.org/10.1021/acs.jpclett.6b00384.

[115] Saha P, Datta MK, Velikokhatnyi OI, Manivannan A, Alman D, Kumta PN. Rechargeable magnesium battery: current status and key challenges for the future. Prog Mater Sci 2014;66:1–86. https://doi.org/10.1016/j.pmatsci.2014.04.001.

[116] Yoo HD, Shterenberg I, Gofer Y, Gershinsky G, Pour N, Aurbach D. Mg rechargeable batteries: an on-going challenge. Energy Environ Sci 2013;6:2265–79. https://doi.org/10.1039/c3ee40871j.

[117] Yagi S, Tanaka A, Ichikawa Y, Ichitsubo T, Matsubara E. Effects of water content on magnesium deposition from a Grignard reagent-based tetrahydrofuran electrolyte. Res Chem Intermed 2014;40:3–9. https://doi.org/10.1007/s11164-013-1449-9.

[118] Gregory TD, Hoffman RJ, Winterton RC. Nonaqueous electrochemistry of magnesium: applications to energy storage. J Electrochem Soc 1990;137:775–80. https://doi.org/10.1149/1.2086553.

[119] Gao X, Mariani A, Jeong S, Liu X, Dou X, Ding M, Moretti A, Passerini S. Prototype rechargeable magnesium batteries using ionic liquid electrolytes. J Power Sources 2019;423:52–9. https://doi.org/10.1016/j.jpowsour.2019.03.049.

[120] NuLi Y, Yang J, Wu R. Reversible deposition and dissolution of magnesium from BMIMBF4 ionic liquid. Electrochem Commun 2005;7:1105–10. https://doi.org/10.1016/j.elecom.2005.07.013.

[121] Zhan Y, Zhang W, Lei B, Liu H, Li W. Recent development of Mg ion solid electrolyte. Front Chem 2020;8:1–7. https://doi.org/10.3389/fchem.2020.00125.

[122] Chusid O, Gofer Y, Gizbar H, Vestfrid Y, Levi E, Aurbach D, Riech I. Solid-state rechargeable magnesium batteries. Adv Mater 2003;15:627–30. https://doi.org/10.1002/adma.200304415.

[123] Jaschin PW, Gao Y, Li Y, Bo SH. A materials perspective on magnesium-ion-based solid-state electrolytes. 2020. https://doi.org/10.1039/c9ta11729f.

[124] Ikeda S, Takahashi M, Ishikawa J, Ito K. Solid electrolytes with multivalent cation conduction. 1. Conducting species in Mg Zr PO4 system. Solid State Ionics 1987;23:125–9. https://doi.org/10.1016/0167-2738(87)90091-9.

[125] Komarneni S, Agrawal D, Roy R. [MgZrn(P04) 6], vol. 23; 1988. p. 5–7.

[126] Nakano K, Noda Y, Tanibata N, Nakayama M, Kajihara K, Kanamura K. Computational investigation of the Mg-ion conductivity and phase stability of MgZr4(PO4)6. RSC Adv 2019;9:12590–5. https://doi.org/10.1039/c9ra00513g.

[127] Imanaka N, Okazaki Y, Adachi GY. Divalent magnesium ion conducting characteristics in phosphate based solid electrolyte composites. J Mater Chem 2000;10:1431–5. https://doi.org/10.1039/a909599c.

[128] Imanaka N, Okazaki Y, Adachi G. Divalent magnesium ionic conduction in Mg 1-2x(Zr 1-xNb x) 4P 6O 24 (x = 0-0.4) solid solutions. Electrochem Solid State Lett 2000;3:327–9. https://doi.org/10.1149/1.1391138.

[129] Imanaka N, Okazaki Y, Adachi G. Optimization of divalent magnesium ion conduction in phosphate based polycrystalline solid electrolytes. Ionics 2001;7:440–6. https://doi.org/10.1007/BF02373581.

[130] Tamura S, Yamane M, Hoshino Y, Imanaka N. Highly conducting divalent Mg2+ cation solid electrolytes with well-ordered three-dimensional network structure. J Solid State Chem 2016;235:7–11. https://doi.org/10.1016/j.jssc.2015.12.008.

[131] Halim ZA, Adnan SBRS, Mohamed NS. Effect of sintering temperature on the structural, electrical and electrochemical properties of novel Mg0.5Si2 (PO4)3 ceramic electrolytes. Ceram Int 2016;42:4452–61. https://doi.org/10.1016/j.ceramint.2015.11.131.

[132] High-temperature conductivity measurements of magnesium-ion-conducting solid oxide Mg0.5 x(Zr1 xNbx)2(PO4)3 (x = 0.15) using Mg metal Electrodes. pdf, [n.d.)].

[133] Liang B, Keshishian V, Liu S, Yi E, Jia D, Zhou Y, Kieffer J, Ye B, Laine RM. Processing liquid-feed flame spray pyrolysis synthesized Mg0.5Ce0.2Zr1.8(PO4)3 nanopowders to free standing thin films and pellets as potential electrolytes in all-solid-state Mg batteries. Electrochim Acta 2018;272:144–53. https://doi.org/10.1016/j.electacta.2018.04.015.

[134] Mustafa M, Rani MSA, Adnan SBRS, Salleh FM, Mohamed NS. Characteristics of new Mg0.5(Zr1-xSnx)2(PO4)3 NASICON structured compound as solid electrolytes. Ceram Int 2020;46:28145–55. https://doi.org/10.1016/j.ceramint.2020.07.313.

[135] Anuar NK, Mohamed NS. Structural and electrical properties of novel Mg0.9+ 0.5yZn0.4AlyZr1.6 y(PO4)3 ceramic electrolytes synthesized via nitrate sol–gel method. J Sol Gel Sci Technol 2016;80:249–58. https://doi.org/10.1007/s10971-016-4091-3.

[136] Chłopek K, Frommen C, Léon A, Zabara O, Fichtner M. Synthesis and properties of magnesium tetrahydroborate, Mg(BH4)2. J Mater Chem 2007;17:3496–503. https://doi.org/10.1039/b702723k.

[137] Cuan J, Zhou Y, Zhou T, Ling S, Rui K, Guo Z, Liu H, Yu X. Borohydride-scaffolded Li/Na/Mg fast ionic conductors for promising solid-state electrolytes. Adv Mater 2019;31:1–31. https://doi.org/10.1002/adma.201803533.

[138] Matsuo M, Oguchi H, Sato T, Takamura H, Tsuchida E, Ikeshoji T, Orimo SI. Sodium and magnesium ionic conduction in complex hydrides. J Alloys Compd 2013;580:S98–101. https://doi.org/10.1016/j.jallcom.2013.01.058.

[139] Higashi S, Miwa K, Aoki M, Takechi K. A novel inorganic solid state ion conductor for rechargeable Mg batteries. Chem Commun 2014;50:1320–2. https://doi.org/10.1039/c3cc47097k.

[140] Roedern E, Kühnel RS, Remhof A, Battaglia C. Magnesium ethylenediamine borohydride as solid-state electrolyte for magnesium batteries. Sci Rep 2017;7:2–7. https://doi.org/10.1038/srep46189.

[141] Yan Y, Grinderslev JB, Jørgensen M, Skov LN, rgen Skibsted J, Jensen TR. Ammine magnesium borohydride nanocomposites for all-solid-state magnesium batteries. ACS Appl Energy Mater 2020;3:9264–70. https://doi.org/10.1021/acsaem.0c01599.

[142] Canepa P, Bo SH, Sai Gautam G, Key B, Richards WD, Shi T, Tian Y, Wang Y, Li J, Ceder G. High magnesium mobility in ternary spinel chalcogenides. Nat Commun 2017;8:1–8. https://doi.org/10.1038/s41467-017-01772-1.

[143] Kamaya N, Homma K, Yamakawa Y, Hirayama M, Kanno R, Yonemura M, Kamiyama T, Kato Y, Hama S, Kawamoto K, Mitsui A. A lithium superionic conductor. Nat Mater 2011;10:682–6. https://doi.org/10.1038/nmat3066.

[144] Canepa P, Sai Gautam G, Broberg D, Bo SH, Ceder G. Role of point defects in spinel Mg chalcogenide conductors. Chem Mater 2017;29:9657–67. https://doi.org/10.1021/acs.chemmater.7b02909.

[145] Kundu S, Solomatin N, Kauffmann Y, Kraytsberg A, Ein-Eli Y. Revealing and excluding the root cause of the electronic conductivity in Mg-ion MgSc2Se4 solid electrolyte. Appl Mater Today 2021;23:100998. https://doi.org/10.1016/j.apmt.2021.100998.

[146] Bekaert E, Buannic L, Lassi U, Llordés A, Salminen J. Electrolytes for Li- and Na-ion batteries: concepts, candidates, and the role of nanotechnology. Elsevier Inc.; 2017. https://doi.org/10.1016/B978-0-323-42977-1.00001-7.

[147] Ye L, Feng Z. Polymer electrolytes as solid solvents and their applications, Polymer Electrolytes: fundamentals and Applications. 2010. p. 550–82. https://doi.org/10.1533/9781845699772.2.550.

[148] Acosta JL, Morales E. Synthesis and characterization of polymeric electrolytes for solid state magnesium batteries. Electrochim Acta 1997;43:791–7. https://doi.org/10.1016/S0013-4686(97)00123-0.

[149] Liebenow C. A novel type of magnesium ion conducting polymer electrolyte. Electrochim Acta 1998;43:1253–6. https://doi.org/10.1016/S0013-4686(97)10026-3.

[150] Girish Kumar G, Munichandraiah N. A gel polymer electrolyte of magnesium triflate. Solid State Ionics 2000;128:203–10. https://doi.org/10.1016/s0167-2738(00)00276-9.

[151] Girish Kumar G, Munichandraiah N. Solid-state rechargeable magnesium cell with poly(vinylidenefluoride)-magnesium triflate gel polymer electrolyte. J Power Sources 2001;102:46–54. https://doi.org/10.1016/S0378-7753(01)00772-8.

[152] Yoshimoto N, Yakushiji S, Ishikawa M, Morita M. Rechargeable magnesium batteries with polymeric gel electrolytes containing magnesium salts. Electrochim Acta 2003;48:2317–22. https://doi.org/10.1016/S0013-4686(03)00221-4.

[153] Pandey GP, Hashmi SA. Experimental investigations of an ionic-liquid-based, magnesium ion conducting, polymer gel electrolyte. J Power Sources 2009;187:627–34. https://doi.org/10.1016/j.jpowsour.2008.10.112.

[154] Saito M, Ikuta H, Uchimoto Y, Wakihara M, Yokoyama S, Yabe T, Yamamoto M. Interaction between the Lewis acid group of a borate ester and various anion species in a polymer electrolyte containing Mg salt. J Phys Chem B 2003;107:11608–14. https://doi.org/10.1021/jp034040b.

[155] Thelen JL, Inceoglu S, Venkatesan NR, Mackay NG, Balsara NP. Relationship between ion dissociation, melt morphology, and electrochemical performance of lithium and magnesium single-ion conducting block copolymers. Macromolecules 2016;49:9139–47. https://doi.org/10.1021/acs.macromol.6b01886.

[156] Merrill LC, Ford HO, Schaefer JL. Application of single-ion conducting gel polymer electrolytes in magnesium batteries. ACS Appl Energy Mater 2019;2:6355–63. https://doi.org/10.1021/acsaem.9b00991.

[157] Polu AR, Kumar R, Rhee H. Magnesium ion conducting solid polymer blend electrolyte based on biodegradable polymers and application in solid-state batteries. 2014. https://doi.org/10.1007/s11581-014-1174-4.

[158] Polu AR, Kumar R. Ionic conductivity and discharge characteristic studies of PVA-Mg (CH 3 COO) 2 solid polymer electrolytes ionic conductivity and discharge characteristic studies of PVA-Mg (CH 3 COO) 2 solid polymer electrolytes, vol. 4037; 2013. https://doi.org/10.1080/00914037.2012.664211.

[159] Anilkumar KM, Jinisha B, Manoj M, Jayalekshmi S. Poly (ethylene oxide) (PEO) - poly (vinyl pyrrolidone) (PVP) blend polymer based solid electrolyte membranes for developing solid state magnesium ion cells. Eur Polym J 2017;89:249–62. https://doi.org/10.1016/j.eurpolymj.2017.02.004.

[160] Kamarudin KH, Sheng CK. Solid polymer electrolytes based on starch-Magnesium Sulphate: study on morphology and electrical conductivity. 2018.

[161] Ponraj T, Ramalingam A, Selvasekarapandian S, Srikumar SR, Manjuladevi R. Plasticized solid polymer electrolyte based on triblock copolymer poly(vinylidene chloride-co-acrylonitrile-co-methyl methacrylate) for magnesium ion batteries. Polym Bull 2021;78:35–57. https://doi.org/10.1007/s00289-019-03091-5.

[162] Wang T, Zhao X, Liu F, Fan LZ. Porous polymer electrolytes for long-cycle stable quasi-solid-state magnesium batteries. J Energy Chem 2021;59:608–14. https://doi.org/10.1016/j.jechem.2020.12.004.

[163] Kumar GG, Munichandraiah N. Solid-state rechargeable magnesium cell with poly (vinylidene¯uoride)±magnesium tri¯ate gel polymer electrolyte. J Power Sources 2001:9.

[164] Patel S, Kumar R. Synthesis and characterization of magnesium ion conductivity in PVDF based nanocomposite polymer electrolytes disperse with MgO. J Alloys Compd 2019;789:6–14. https://doi.org/10.1016/j.jallcom.2019.03.089.

[165] Manjuladevi R, Thamilselvan M, Selvasekarapandian S, Mangalam R, Premalatha M, Monisha S. Mg-ion conducting blend polymer electrolyte based on poly(vinyl alcohol)-poly (acrylonitrile) with magnesium perchlorate. Solid State Ionics 2017;308:90–100. https://doi.org/10.1016/j.ssi.2017.06.002.

[166] Sundar M, Selladurai S. Effect of fillers on magnesium – poly (ethylene oxide) solid polymer electrolyte. 2006. p. 281–6. https://doi.org/10.1007/s11581-006-0048-9.

[167] Polu AR, Kumar R, Kumar KV, Jyothi NK. Ceramic filler on PEG-based composite polymer electrolytes for magnesium batteries effect of TiO 2 ceramic filler on PEG-based composite polymer electrolytes for magnesium batteries, 996; 2013. p. 996–8. https://doi.org/10.1063/1.4791378.

[168] Song S, Kotobuki M, Zheng F, Li Q, Xu C, Wang Y, Li WDZ, Hu N, Lu L. Communication — a composite polymer electrolyte for safer Mg. Batteries 2017;164:741–3. https://doi.org/10.1149/2.1171704jes.

[169] Pandey GP, Agrawal RC, Hashmi SA. Magnesium ion-conducting gel polymer electrolytes dispersed with fumed silica for rechargeable magnesium battery application. 2011. p. 2253–64. https://doi.org/10.1007/s10008-010-1240-4.

[170] Pandey GP, Agrawal RC, Hashmi SA. Magnesium ion-conducting gel polymer electrolytes dispersed with nanosized magnesium oxide, vol. 190; 2009. p. 563–72. https://doi.org/10.1016/j.jpowsour.2009.01.057.

[171] Shao Y, Nidhi N, Hu J, Hu M, Liu T, Wei Z, Gu M, Deng X, Xu S, Sung K, Wang J, Nie Z, Li G, Zavadil KR, Xiao J, Wang C, Henderson WA, Zhang J, Wang Y, Mueller KT, Persson K, Liu J. Nanocomposite polymer electrolyte for rechargeable magnesium batteries. Nano Energy 2015;12:750–9. https://doi.org/10.1016/j.nanoen.2014.12.028.

[172] Du A, Zhang H, Zhang Z, Zhao J, Cui Z, Zhao Y, Dong S, Wang L, Zhou X, Cui G. A crosslinked polytetrahydrofuran-borate-based polymer electrolyte enabling wide-working-temperature-range rechargeable magnesium batteries. Adv Mater 2019;31:1–7. https://doi.org/10.1002/adma.201805930.

[173] Sun J, Zou Y, Gao S, Shao L, Chen C. Robust strategy of quasi-solid-state electrolytes to boost the stability and compatibility of Mg ion batteries. ACS Appl Mater Interfaces 2020;12:54711–9. https://doi.org/10.1021/acsami.0c16204.

[174] Wu K, Huang J, Yi J, Liu X, Liu Y, Wang Y, Zhang J, Xia Y. Recent advances in polymer electrolytes for zinc ion batteries: mechanisms, properties, and perspectives. Adv Energy Mater 2020;10:1903977. https://doi.org/10.1002/aenm.201903977.

[175] Ye Z, Cao Z, Lam Chee MO, Dong P, Ajayan PM, Shen J, Ye M. Advances in Zn-ion batteries via regulating liquid electrolyte. Energy Storage Mater 2020;32:290–305. https://doi.org/10.1016/j.ensm.2020.07.011.

[176] An Y, Tian Y, Zhang K, Liu Y, Liu C, Xiong S, Feng J, Qian Y. Stable Aqueous anode-free zinc batteries enabled by interfacial engineering. Adv Funct Mater 2021;31:2101886. https://doi.org/10.1002/adfm.202101886.

[177] Han S-D, Rajput NN, Qu X, Pan B, He M, Ferrandon MS, Liao C, Persson KA, Burrell AK. Origin of electrochemical, structural, and transport properties in nonaqueous zinc electrolytes. ACS Appl Mater Interfaces 2016;8:3021–31. https://doi.org/10.1021/acsami.5b10024.

[178] Blanc LE, Kundu D, Nazar LF. Scientific challenges for the implementation of Zn-ion batteries. Joule 2020;4:771–99. https://doi.org/10.1016/j.joule.2020.03.002.

[179] Li H, Han C, Huang Y, Huang Y, Zhu M, Pei Z, Xue Q, Wang Z, Liu Z, Tang Z, Wang Y, Kang F, Li B, Zhi C. An extremely safe and wearable solid-state zinc ion battery based on a hierarchical structured polymer electrolyte. Energy Environ Sci 2018;11:941–51. https://doi.org/10.1039/C7EE03232C.

[180] Krauskopf T, Richter FH, Zeier WG, Janek J. Physicochemical concepts of the lithium metal anode in solid-state batteries. Chem Rev 2020;120:7745–94. https://doi.org/10.1021/acs.chemrev.0c00431.

[181] Wang M, Emre A, Tung S, Gerber A, Wang D, Huang Y, Cecen V, Kotov NA. Biomimetic solid-state Zn2+ electrolyte for corrugated structural batteries. ACS Nano 2019;13:1107–15. https://doi.org/10.1021/acsnano.8b05068.

[182] Rathika R, Padmaraj O, Suthanthiraraj SA. Electrical conductivity and dielectric relaxation behaviour of PEO/PVdF-based solid polymer blend electrolytes for zinc battery applications. Ionics 2018;24:243–55. https://doi.org/10.1007/s11581-017-2175-x.

[183] Karan S, Sahu M, Sahu TB, Mahipal YK, Sahu DK, Agrawal RC. Investigations on materials and ion transport properties of Zn2+ conducting nano-composite polymer electrolytes (NCPEs): [(90 PEO: 10 Zn(CF3SO3)2)+ x ZnO]. Mater Today Commun 2017;13:269–74. https://doi.org/10.1016/j.mtcomm.2017.10.009.

[184] Wang Z, Hu J, Han L, Wang Z, Wang H, Zhao Q, Liu J, Pan F. A MOF-based single-ion Zn2+ solid electrolyte leading to dendrite-free rechargeable Zn batteries. Nano Energy 2019;56:92–9. https://doi.org/10.1016/j.nanoen.2018.11.038.

[185] Ma L, Chen S, Li N, Liu Z, Tang Z, Zapien JA, Chen S, Fan J, Zhi C. Hydrogen-free and dendrite-free all-solid-state Zn-ion batteries. Adv Mater 2020;32:1908121. https://doi.org/10.1002/adma.201908121.

[186] Liu C, Xie X, Lu B, Zhou J, Liang S. Electrolyte strategies toward better zinc-ion batteries. ACS Energy Lett 2021;6:1015–33. https://doi.org/10.1021/acsenergylett.0c02684.

[187] Mo F, Chen Z, Liang G, Wang D, Zhao Y, Li H, Dong B, Zhi C. Zwitterionic sulfobetaine hydrogel electrolyte building separated positive/negative ion migration channels for aqueous Zn-MnO2 batteries with superior rate capabilities. Adv Energy Mater 2020;10:2000035. https://doi.org/10.1002/aenm.202000035.

[188] Li Q, Cui X, Pan Q. Self-healable hydrogel electrolyte toward high-performance and reliable quasi-solid-state Zn–MnO2 batteries. ACS Appl Mater Interfaces 2019;11:38762–70. https://doi.org/10.1021/acsami.9b13553.

[189] Mo F, Liang G, Meng Q, Liu Z, Li H, Fan J, Zhi C. A flexible rechargeable aqueous zinc manganese-dioxide battery working at 20 °C. Energy Environ Sci 2019;12:706–15. https://doi.org/10.1039/C8EE02892C.

[190] Mo F, Li H, Pei Z, Liang G, Ma L, Yang Q, Wang D, Huang Y, Zhi C. A smart safe rechargeable zinc ion battery based on sol-gel transition electrolytes. Sci Bull 2018;63:1077–86. https://doi.org/10.1016/j.scib.2018.06.019.

[191] Li C, Hou C-C, Chen L, Kaskel S, Xu Q. Rechargeable Al-ion batteries. Energy 2021;3:100049. https://doi.org/10.1016/j.enchem.2020.100049.

[192] Yu Z, Jiao S, Tu J, Song W-L, Lei H, Jiao H, Chen H, Fang D. Gel electrolytes with a wide potential window for high-rate Al-ion batteries. J Mater Chem A 2019;7:20348–56. https://doi.org/10.1039/C9TA06815E.

[193] Kim I, Jang S, Lee KH, Tak Y, Lee G. In situ polymerized solid electrolytes for superior safety and stability of flexible solid-state Al-ion batteries. Energy Storage Mater 2021;40:229–38. https://doi.org/10.1016/j.ensm.2021.05.019.

[194] Yu Z, Jiao S, Li S, Chen X, Song W-L, Teng T, Tu J, Chen H-S, Zhang G, Fang D-N. Flexible stable solid-state Al-ion batteries. Adv Funct Mater 2019;29:1806799. https://doi.org/10.1002/adfm.201806799.